REPORT DOCUMENTATION PAGE

Form Approved
OMB NO. 0704-0188

1. AGENCY USE ONLY (Leave Blank)	2. REPORT DATE **9/29/04**	3. REPORT TYPE AND DATES COVERED **Final Technical 07/01/03 – 6/30/04**

4. TITLE AND SUBTITLE
Multiple Antenna Communication with Time Reversal Mirror (MIMO-TRM) Pre-Processing

5. FUNDING NUMBERS
Grant No: N00014-03-0906

6. AUTHOR(S)
Professor Arogyaswami J. Paulraj

7. PERFORMING ORGANIZATION NAME(S) AND ADDRESS(ES)
Stanford University
Electrical Engineering Department
Stanford, CA 94305

8. PERFORMING ORGANIZATION REPORT NUMBER

9. SPONSORING / MONITORING AGENCY NAME(S) AND ADDRESS(ES)
Wen C. Masters
Office of Naval Research
Ballston Center Tower One
800 N. Qunicy Street
Arlington, VA 22217-5660

10. SPONSORING / MONITORING AGENCY REPORT NUMBER
Office of Naval Research
1107 N.E. 45th St., Suite 350
Seattle, WA 98105-4631

11. SUPPLEMENTARY NOTES
The views, opinions and/or findings contained in this report are those of the author(s) and should not be construed as an official Department of the Army position, policy or decision, unless so designated by other documentation.

12 a. DISTRIBUTION / AVAILABILITY STATEMENT
Approved for public release; distribution unlimited.

12 b. DISTRIBUTION CODE

13. ABSTRACT (Maximum 200 words)

We have pioneered the study of time reversal (TR) pre-processing in radio wireless communication. Our results have shown that TR is beneficial for use in a rich scattering environment with many propagation paths, thus positioning the technique as a low complexity solution for high data rate communication via large delay spread channels. Methods to improve the performance of TR have been studied, and comparisons with other precoding schemes have been made. In particular, a TR system prototype has been designed, and is being built for carrying out future experiments.

15. NUMBER OF PAGES
3

16. PRICE CODE

17. SECURITY CLASSIFICATION OR REPORT	18. SECURITY CLASSIFICATION ON THIS PAGE	19. SECURITY CLASSIFICATION OF ABSTRACT	20. LIMITATION OF ABSTRACT
UNCLASSIFIED	**UNCLASSIFIED**	**UNCLASSIFIED**	**UL**

NSN 7540-01-280-5500

Standard Form 298 (Rev.2-89)
Prescribed by ANSI Std. 239-18

Enclosure 1

Multiple Antenna Communication with Time Reversal Mirror (MIMO-TRM) Pre-Processing

Abstract

We have pioneered the study of time reversal (TR) pre-processing in radio wireless communication. Our results have shown that TR is beneficial for use in a rich scattering environment with many propagation paths, thus positioning the technique as a low complexity solution for high data rate communication via large delay spread channels. Methods to improve the performance of TR have been studied, and comparisons with other precoding schemes have been made. In particular, a TR system prototype has been designed, and is being built for carrying out future experiments.

Introduction

Communication via a large delay spread channel at high data rate has proven to be a challenging task, primarily due to the substantial amount of intersymbol interference (ISI) incurred by the long channel impulse response (CIR). Time reversal (TR) is a simple pre-processing technique that makes such communication feasible without the need for any complex receivers. In a TR communication system, the receiver first sends a training sequence to the transmitter for channel estimation. The transmitter convolves the message with the time-reversed CIR, and sends it to the receiver. Three main benefits result from this simple transmission scheme.

- Spatial focusing – The spatial profile of the received signal's power peaks at the receiver and decays rapidly away from the receiver. This means that co-channel interference in a multi-cell system is low, and the probability of interception by an unintended receiver is small. As a result, efficient frequency reuse can be realized, and secure communication is attained.
- Temporal focusing – Analogous to traditional matched filtering at the receiver, the power of all multipaths in the CIR can be collected at one particular time instant. Thus, the receiver can detect the transmitted message at this time instant with maximum signal-to-noise ratio (SNR).
- Channel hardening – The time variation of the effective CIR seen by the receiver is significantly less than that of the original channel. In other words, a high frequency diversity gain is achieved, and the adverse effect of fading is reduced.

Although TR has been studied extensively, and applied successfully, in the ultrasound and underwater acoustic arenas, especially in a rich scattering environment with ample multipaths, its suitability for wireless radio has yet to be determined. The core of our research activities was to investigate the feasibility of applying TR to high data rate wireless radio communication. The research results are summarized in the following section. For detailed explanations, please refer to the attached publications.

Summary of Research Results

1. M. Emami, J. Hansen, A. Kim, G. Papanicolaou, A. Paulraj, D. Cheung, and C. Prettie, "Predicted Time Reversal Performance in Wireless Communications Using Channel Measurements," to appear in IEEE Communications Letters.

This work represents the first effort in estimating the performance of TR in wireless radio using real channel measurements. Data were taken in an indoor environment in the 2 to 8 GHz frequency band by Intel Corporation. Our calculations show that the 3 main benefits of TR, namely spatial focusing, temporal focusing and channel hardening, can all be obtained. These results support the theory that TR is an equally attractive technology for wireless radio communication as for ultrasound and underwater acoustic communication.

2. J. Hansen, D. Baum, A. Paulraj, "Design Approach for a Time Reversal Test Bed for Radio Channels," Special Session on MIMO Prototyping, 12th European Signal Processing Conference, Sept. 2004.

This work describes the design of a prototype system for carrying out TR experiments in wireless radio. The design is heavily based on an off-the-shelf multiple-input-multiple-output (MIMO) channel sounder, in order to keep implementation and development costs low. A company has tentatively agreed to build this prototype, pending final approval of contract by Stanford University and the company. The availability of this prototype will allow us to demonstrate that the predicted benefits of TR can actually be attained in practical environments.

3. T. Strohmer, M. Emami, J. Hansen, G. Papanicolaou, A. Paulraj, "Application of Time Reversal with MMSE Equalizer to UWB Communications," Global Telecommunications Conference, Dec. 2004.

This work examines the performance gain of adding a minimum mean square error (MMSE) linear equalizer at the receiver of a TR system. Performance improvement is obtained because ISI still exists in the received signal, even though the signal is already time compressed. Moreover, for fixed equalizer complexity, the concept of rate-backoff is introduced. The idea is to reduce the transmission rate, and hence the ISI, to a point such that a certain performance level is maintained.

4. M. Emami, M. Vu, J. Hansen, A. Paulraj, G. Papanicolaou, "Matched Filtering with Rate Back-off for Low Complexity Communications in Very Large Delay Spread Channels," submitted to Asilomar Conference on Signals, Systems, and Computers, Nov. 2004. (Extended Abstract)

This work derives the optimum MMSE linear prefilter for an ISI channel, subject to the constraint of a simple, one-tap equalizer at the receiver. The performance of this transmission strategy is compared to that of TR.

5. C. Oestges, J. Hansen, M. Emami, A. Paulraj, G. Papanicolaou, "Time Reversal Techniques for Broadband Wireless Communications," European Microwave Week, Oct. 2004. (Invited Paper)

This paper gives an overview of the TR technology as applied to wireless radio communication. It contains both a tutorial introduction and recent research results, including results discussed in the above contributions.

Conclusions and Future Work

We have initiated the investigation on applying TR to wireless radio communication. Our results have shown that TR is a promising technology to pursue, with the capability of achieving high data rate at low complexity under hostile environment with large amount of ISI. Future research will continue to examine TR in details. Questions such as how inaccurate channel information affects performance, and how spatial focusing can be quantitatively measured, will be addressed. Comparisons with nonlinear precoding techniques will also be made. Moreover, we expect to perform TR experiments in practical environments once our prototype system is available. On a broader perspective, we seek to better understand the fundamental tradeoff between spectral efficiency, power consumption, performance and complexity when communicating via large delay spread channels at high data rate.

DESIGN APPROACH FOR A TIME REVERSAL TEST BED FOR RADIO CHANNELS

— SPECIAL SESSION ON MIMO PROTOTYPING —

J. Hansen[1], *D. S. Baum*[2], *and A. Paulraj*[1]

[1] Information Systems Lab, Stanford University, Stanford, CA, USA
phone: +1 650 723 0711, fax: +1 650 723 8473, email: {jchansen,apaulraj@stanford.edu}
[2] Communication Technology Lab, Swiss Federal Institute of Technology (ETH) Zürich, Zürich, Switzerland
phone: +41 1 632 2791, fax: +41 1 632 1209, email: dsbaum@nari.ee.ethz.ch

ABSTRACT

In time reversal, a message signal to be transmitted is first convolved with the time-reversed channel impulse response and then sent to the receiver. The "time-reversed" waves which propagate into the channel retrace their former paths; they eventually lead to a focus of power in space and time at the receiver. Time reversal systems can use antenna arrays in order to enhance the focusing, but they do not necessarily need to. The channel's degrees of freedom are rather excited by using broadband signals, and the focusing can be achieved with single-antenna links.

To the authors' best knowledge, there has been no demonstration of time reversal in wireless radio yet. This paper describes the broad design principles of a system that is designed to demonstrate time reversal in wireless radio channels. The system block diagram, some critical specifications and sources of error are described. Experimental data will be presented, if available in time, at the workshop.

1. INTRODUCTION

In a practical system employing time reversal (TR), an intented receiver sends a training sequence to an intended transmitter which is equipped with one or potentially more than one transmit antenna. The transmitter time-reverses the estimated channel impulse response (CIR) and convolves this signal with any message signal that is then sent to the receiver.

In quasi-static, reciprocal channels this simple precoding scheme yields a concentration of power at only the intended receiver at a particular time. The spatial and temporal focusing that can be achieved by TR has been successfully demonstrated in ultra-sound by Fink [1, 2] and in underwater acoustics [2, 3, 4, 5].

In wireless communications, no demonstration is known to the authors. In this paper, we propose to convert a commerically available broadband MIMO channel sounder into a device that can demonstrate the leverage of TR in low Doppler (quasi time-invariant) channels with about one microsecond delay spread. Our strategy is to keep the upgrade as simple as possible. We rely on the MIMO sounder's capability for channel estimation, and add the features to transfer the CIR estimates back to the transmitter via an external link and to then transmit a precoded message. Hence, we replace the pair of transceivers usually considered in TR experiments by a single transmitter and a single receiver which are connected by some feedback loop. The TR sounder is designed such that this feedback loop can be chosen from a variety of publicly available, wired or wireless, links.

The rationals for this strategy are twofold. For one, the modification of this type of existing and verified system minimizes the amount of additional hardware effort needed and the risk of system performance failure. Secondly, the usage of the same link for channel estimation and TR eliminates any problems with the reciprocity assumptions that possibly occur due to differences in transmit and receiver RF chains of a single transceiver.

The remainder of the paper is organized as follows. In the next section, we give a brief introduction to TR. In the third section, we describe the system's design principles. We proceed to investigate critial specifications and sources of error in the fourth, and conclude in the fifth section.

2. TIME REVERSAL

The transmitter uses the time-reversed complex conjugate of the CIR as the transmit prefilter. We denote the CIR by $h(\mathbf{r}_0, \tau)$, where $\mathbf{r}_0$ is the receiver location and τ is the delay variable. Applying $h^*(\mathbf{r}_0, -\tau)$ as the prefilter, the effective channel to any location $\mathbf{r}$ is thus given by the time-reversed field

$$s(\mathbf{r}, \tau) \triangleq \mathbf{h}^*(\mathbf{r}_0, -\tau) \otimes \mathbf{h}(\mathbf{r}, \tau) \qquad (1)$$

where "$\otimes$" denotes convolution.

A convolution with a time-reversed signal is equivalent to a correlation. We see from (1) that the focusing relies on the decorrelation of CIRs in the delay and the spatial domain. A CIR can be considered a random code sequence that is assigned to a transmit-receive pair. The auto- and crosscorrelation properties of this sequence are given by nature. In contrast to CDMA, they come without any additional bandwidth spreading. The decorrelation of the CIRs is obviously best in a rich scattering environment. In addition, high bandwidths unleash the channel's degrees of freedom and aid decorrelation. Physically, one can consider the ubiquitous locations of the scatterers to form a large virtual aperture which enables focusing even with a single antenna down to the diffraction limit. A simple but effective measure for the focusing capability of a TR channel is the delay-spread bandwidth product which roughly gives the number of taps that the CIRs has. For an initial evaluation of the benefits of TR we refer to [6].

3. SOUNDER ARCHITECTURE

The commercially available MIMO sounding unit consists of the following parts. The transmitter contains a signal generating unit (SGTx) and a transmitter RF module (RFTx), the

Jan Hansen's work was supported by the grant HA3499/1-1 of the Deutsche Forschungsgemeinschaft (DFG).

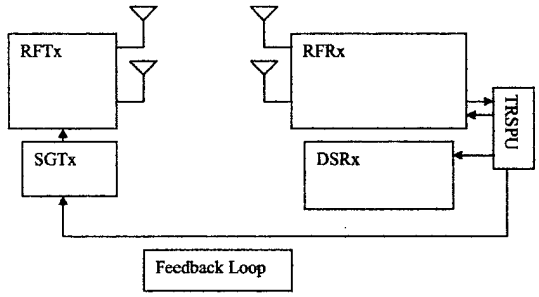

Figure 1: A schematic of the TR sounder.

receiver contains a receiver RF module (RFRx) and a data storage unit (DSRx). The conversion of this sounder into a TR sounder is done by adding components which we call TR signal processing unit (TRSPU) and feedback loop (FL). Fig. 1 shows the architecture of the TR sounder.

The proposed TR scheme operates in three steps; the main function of the TRSPU is the flexible definition and coordination of these steps. In a first step, called channel estimation step (CES), the transmitter transmits a training sequence that the receiver uses to estimate the channel. This estimate is time-reversed in the second step, convolved with the transmit sequences, and sent back to the transmitter via the FL. Then, in a third step called time reversal step (TRS), the transmitter transmits the time-reversed sequence into the channel; the receiver now sees a signal that is focused in space and time. The time focusing can be demonstrated by the compressed CIR at the intended receive antenna; the spatial focusing appears because apart from this one antenna, all other ones will detect signals that look like noise.

In the next subsections we describe the specifications of the TR sounder in more detail.

3.1 MIMO Sounding Unit and Antennas

3.1.1 Bandwidth, Carrier Frequency, and Output Power

The maximum bandwidth of the currently available system is 120 MHz. For a delay spread in the range of up to 1 μs, we can hence expect a time bandwidth product of up to 100. Under normal conditions, we expect delay-spreads which are a factor of 10 lower than that; hence, the systems works with a time bandwidth product of about 10 which still suffices to achieve a reasonable benefit with TR.

The carrier frequency of the system is in the ISM band at 2.4 GHz. Unfortunately, the available transmsission bandwidth is limited to 83 MHz. According to FCC regulations on RF devices [7], the maximum allowed EIRP is 4 W, the maximum transmit power is 1 W. The additional 6 dB can be achieved by a suitable choice of transmit antenna.

A second suitable choice would be the ISM band at 5.8 GHz with an available bandwidth of 150 MHz. However, as the free space attenuation is higher and thus reduces transmission range, we decided to perform the demonstration at the lower carrier frequency.

The output power of the system is limited to 1 W.

3.1.2 Signaling

The sounding signals, and in particular their power and power spectral density distribution, are designed in frequency domain. The signals used for channel estimation have constant maximum amplitude over frequency and their phase is designed to minimize the crest factor and hence maximize average output power. Since all signal processing is performed in frequency domain, instead of estimating and time-reversing the CIR, the transfer function (TF) is complex conjugated in frequency domain.

3.1.3 Antennas and Switching

In our system, the antenna elements in an array of the sounder are switched. In this case the number of channels is essentially limited by the number of available switches and antennas and the maximum measurement time for which the quasi-static channel assumption still holds. For the TR experiments, arrays with 4 and 8 antennas will be employed.

Since TR requires a large angular spread, omnidirectional antennas are most advantageous. However, the range that is reqiured to be large in order to obtain a large delay spread would benefit from high gain antennas. The compromise between these two constraints are basestation type transmit antennas (very narrow vertical and wide horizontal beamwidth, gain about 12dBi) and slightly directional antennas (very wide horizontal and wide vertical beamwidth, gain of 6 to 10 dB).

3.1.4 Synchronization

The synchronization is done by using very stable reference clocks at 10 MHz (e.g. Rubidium standards). The clock signal guarantees long term stability. In each RF unit, the carrier signal is generated independently by low-noise PLLs.

3.2 Feedback Loop

In between the CES and the TRS, the estimated channel data has to be transferred from the receiver to the transmitter. The transferral time must be much shorter than the coherence time of the channel. The data rate of the link becomes hence a critical parameter. A single complex CIR with about 1000 taps and 8 bit resolution has a size of about 16 kbit. Assuming a time invariant channel with Doppler frequency of 1 Hz, a realistic transmission time should not be longer than 0.2 s; consequently, the FL needs a data rate of at least 80 kbit/s per CIR that is transferred.

The following options have been evaluated.

3.2.1 Microwave Link

A microwave link is advantageous in terms of data rate, which is in the order of Mbit/s, and in terms of flexibility. Microwave links can be established whereever the experiment is to be performed. However, TR experiments are likely to be conducted in environments with large delay spreads. Here, the TR sounder will operate at maximum EIRP allowed by the FCC regulations. This limit holds for the microwave link, as well. In areas where the SNR of the TR experiment is low, that of the microwave FL is low, too. The link quality can be improved by using directional antennas mounted on high poles, but this requires difficult adjustments and large efforts in the preparation of the experiment.

3.2.2 *Cellular Systems*

Currently available cellular systems such as GPRS offer great flexibility without the need for heavy experimental equipment. Their main drawback is their comparably low data rate (order of 100 kbit/s for GPRS) and, in particular, the unreliable transmission delay. Since the data rate offered does not provide much overhead compared to the data rate required, the application of current cellular services for the FL appears risky, in particular if the Doppler spread of the channel may at times exceed 1 Hz.

3.2.3 *Wired Network*

The wired network offers tremendous data rates; the main drawback is the inflexibility of its access. However, most TR experiments will be conducted in urban areas, where wired access to the internet can be expected to be in range. A wireless network system (WLAN) such as one based on the IEEE 802.11b standard still offers data rates in the order of Mbits and can be employed to bridge the gap between the experimental device to the next wired network connection.

The final decision about the best link depends on the availability of particular services, on local network traffic, and the Doppler spread of the channel. The sounder itself is equipped with RJ45 connectors and can be hooked up to any of the above-mentioned systems.

3.3 The TRSPU

The role of the TRSPU is to coordinate the three steps on which the operation of the sounder is based. Since it also performs the nessecary signal processing, it is located in between the RF and the data storage unit of the receiver.

3.3.1 *The Different TR Modes*

The tasks of a TR sounder are at least threefold: 1) It must demonstrate spatial and temporal focusing when TR experiments are performed with a) a single, or b) multiple transmit antennas. 2) It must be flexible to allow further research about benefits of TR, i.e. for multiuser (MU) communications. 3) It should be backwards compatible. Since it is based on commerical MIMO technology, MIMO channel measurements should still be possible with a TR sounder. It turns out that 4 different TR modes evolve from these requirements:

1. *MIMO Measurements:*
   For MIMO measurements, the TRS is omitted. The sounder performs a predefined number of channel estimations and no TR transmissions.
2. *SISO-TR:*
   In the CES, the channel estimation is performed n_1 times with a single transmit and a single receive antenna. The received TFs can be averaged to obtain a better estimation of the channel. The TRSPU complex conjugates this TF, multiplies it with the Fourier transform of the used transmit sequences, and sends it via the FL to the transmitter. The transmitter loads this sequence and transmits its Fourier-inverse into the channel. Now, in the TRS, the TRSPU provides a second switching table and the RFRx switches through the antenna array. At the one receive antenna that is used in the CES, the detected CIR is compressed. At all other antennas, a noise-like signal appears. After n_2 transmissions, the CES is repeated. This mode is the simplest and best suited to demonstrate TR.

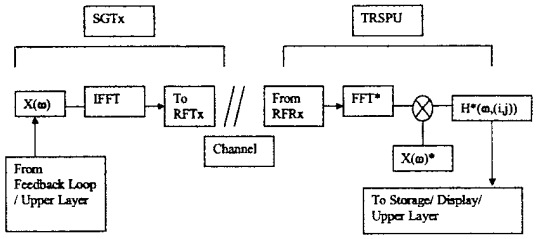

Figure 2: The lower layer of the TRSPU, synchronized with the SGTx.

3. *MU-SIMO-TR:*
   In this mode, MU communication with TR can be demonstrated. The CES is performed with a single transmit antenna and an antenna array at the receiver. Conceptually, it works similar to the SISO-TR mode, except that the TFs of all receive antennas are estimated. The TF estimated at each antenna is multiplied with a message that is to be sent to this antenna; the sum of all these products is fed into the FL and retransmitted in the TR-mode. The channel acts now as a filter; each receive antenna receives only its intended message, and all the other messages as noise.
4. *MISO-TR:*
   In the original underwater acoustic applications, TR is performed with a transmit array. Each transmit antenna focuses its signal on the same receive antenna, so that the focusing is enhanced proportional to the number of transmit antennas. Since in our application, the arrays are switched, the superposition of the signals can only be done by software. Also, the switching requires short-term phase stability at the transmitter.
   This 4th mode is not only the most demanding with respect to synchronization, but also with respect to the data rate on the FL, since as many CIRs must be transferred as there are transmit antennas.

3.3.2 *Double Layered Structure of the TRSPU*

The TRSPU is implemented in a double-layered structure. The lower layer runs synchronized with the SGTx and is as such displayed in Fig. 2. The SGTx receives a sequence from the FL, transforms it into time domain and hands it over to the RFTx. The TRSPU receives the demodulated signal from the RFRx and computes the conjugate of the received CIR via an FFT and division by the sequence used for channel estimation. This layer is run in all modes of the sounder, be it MIMO channel estimation, or one of the two stages of the different TR modes.

The upper layer bascially determines the TR mode, as described in Subsection 3.3.1. Each mode is defined by particular numbers n_1 and n_2 for the duration of the CES and the TRS, and the one (for the MIMO mode) or the two (for all other TR modes) corresponding switching tables that are provided to the RFRx. The upper layer is software-defined. This allows any user to make changes in the setup; in particular, the TR modes can be embedded in more sophisticated high-level transmission schemes, e.g., schemes that adapt the numbers n_1 and n_2 to particular channel conditions.

An example of the SISO-TR mode is shown in Fig. 3. For

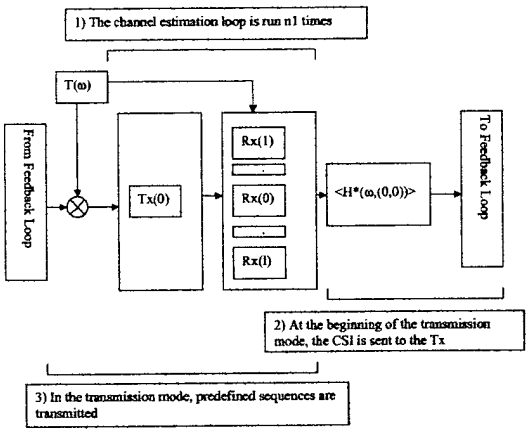

Figure 3: The SISO mode as triggered by the upper layer of the TRSPU.

a given transmit antenna Tx(0) and an intended receive antenna Rx(0), the TF $H(\omega,(0,0))$ is estimated in the first step. In the second step, it is multiplied with the Fourier transform of a transmit sequence and transmitted to the FL. In the third step, the sounder transmits these combined sequences until it again enters the first step.

4. CRITICAL SPECIFICATIONS AND SOURCES OF ERROR

4.1 Range and Power

TR works best in environments with large delay spreads, i.e. over large distances. Consequently, the demands on the link budget are high. The critical parameters are here the pathloss exponent, the maximum and average transmit power determined by hardware and FCC, the bandwidth and the carrier frequency, the antenna gains, the correlation gains, the sounder's sensitivity and the target SNR. Initial computations result in a range of about 600m for the described system with a target SNR of 30 dB in a cluttered environment with a pathloss of $q = 3.5$. This range corresponds to a propagation time of $2\mu s$ which is considered sufficient to create a delay spread of up to $1\mu s$.

4.2 Feedback Loop

The FL is the bottleneck of the sounder. As discussed in Subsection 3.2, the data rate required for the feedback is about 80 kbit times the number of CIRs to be transferred. Depending on the mode, only one CIR, or as many as there are transmit antennas, have to pass the loop.

If links with a data rate in the order of Mbits such as a wired network or a wired network in conjunction with a WLAN are used, the transmission time itself is much shorter than any residuary Doppler of the channel within the observation period. However, other traffic in the network can delay packet transmission. Initial experiments showed that packets of the size of 64 kbit had travel times of about 130 ms on an 11 Mbit WLAN and 20 ms on a local 100 Mbit LAN.

4.3 Phase Noise

TR requires exact phase information at the transmitter. Inaccuracies in the phases occur since a) the channel is not perfectly time variant, b) the LO signals derived by PLLs from the 10 MHz reference have phase noise.

The time variance can be overvome if the data rate of the FL is large enough (Subsection 3.2 and 4.2).

Phase noise destroys the coherent superposition of signals transmitted from multiple antennas. Since it enters both at the transmitter and the receiver, it will reduce the received power by a factor of $\cos({}_{\Delta}\phi_1 + {}_{\Delta}\phi_2)$, where ${}_{\Delta}\phi_i$, $i = 1,2$ are random variables that describe the phase fluctuations of the transmitter's and the receiver's oscillators. For phase errors less than 15°, this yields a performance loss of about 10 % in SNR, which is tolerable. For switched antenna sounders this is less of a problem with respect to TR.

5. CONCLUSIONS

This paper introduces time reversal (TR) as a promising transmission technique for wireless communications. We propose the design of a prototype device that will allow the demonstration of the benefits of TR. This prototype is heavily based on commercially available systems and components, implementation and development costs are kept at a minimum. The core of the device is a commercially available MIMO broadband channel sounder. It can be connected to various types of publicly available networks which serve as a feedback loop. Its key component is the TR signal processing unit, which can operate in several modes and offers flexible handling of the entire device.

REFERENCES

[1] A. Derode, P. Roux, and M. Fink, "Robust acoustic time reversal with high-order multiple scattering," *Phys. Rev. Letters*, vol. 75, pp. 4206–4209, 1995.

[2] A. Derode *et al.*, "Taking advantage of multiple scattering to communicate with time-reversal antennas," *Phys. Rev. Letters*, vol. 90, 2003.

[3] D. Rouseff *et al.*, "Underwater acoustic communication by passive-phase conjugation: Theory and experimental results," *IEEE Journal of Oceanic Engineering*, vol. 26, pp. 821–831, 2001.

[4] M. G. Heinemann, A. Larazza, and K. B. Smith, "Acoustic communications in an enclosure using single-channel time-reversal acoustics," *Appl. Phys. Lett.*, vol. 80, pp. 694–696, 2002.

[5] G. F. Edelmann *et al.*, "An initial demonstration of underwater acoustic communications using time reversal," *IEEE Journal of Oceanic Engineering*, vol. 27, pp. 602–609, 2002.

[6] S. M. Emami, J. Hansen, A. D. Kim, G. Papanicolaou, A. J. Paulraj, D. Cheung, and C. Prettie, "Predicted time reversal performance in wireless communications using channel measurements," *IEEE Communications Letters*, submitted Dec. 2003.

[7] "Code of Federal Regulations," Title 47: Telecommunication, Chapter I - Federal Communications Commission, Part 15: Radio Frequency Devices, Sec. 15.247 and 15.248, Oct. 2003, pp. 751—753.

Application of Time-Reversal with MMSE Equalizer to UWB Communications

Thomas Strohmer[1], *Majid Emami*[2], *Jan Hansen*[2], *George Papanicolaou*[3], *and Arogyaswami J. Paulraj*[2]
[1] Department of Mathematics, University of California, Davis, CA 95616-8633, USA.
Email: strohmer@math.ucdavis.edu
[2] Information Systems Laboratory, Stanford University, Stanford, CA 94305, USA.
Tel: 650-723-4102, Fax: 650-723-8473, Email: {jchansen, memami, apaulraj}@stanford.edu
[3] Department of Mathematics, Stanford University
Email:papanico@math.stanford.edu

Abstract

We propose to apply a technique called time-reversal to UWB communications. In time-reversal a signal is precoded such that it focuses both in time and in space at a particular receiver. Spatial focusing reduces interference to other co-existing systems. Due to temporal focusing, the received power is concentrated within a few taps and the task of equalizer design becomes much simpler than without focusing. Furthermore, temporal focusing allows a large increase in transmission rate compared to schemes that let the impulse response ring out before the next symbol is sent. Our paper introduces time-reversal, investigates the benefit of temporal focusing, and examines the performance of an MMSE-TR equalizer in an UWB channel.

Index Terms

Time Reversal, MMSE Equalization, Ultra-Wideband, Intersymbol Interference

Hansen's work was supported by the Deutsche Forschungsgemeinschaft. This work is partially supported by grants AFOSR F49620-01-1-0465, ONR N00014-02-1-0088, NSF DMS grant 0208568 and by NSF Contracts CCR-0241921, 0241919, ONR Contracts N00014-03-1-0766, N00014-03-1-0906 and Intel Corp.

I. Introduction

Ultra-wideband (UWB) has become a suitable candidate for high-data rate, short range communications. Due to the large operation bandwidth, the resolution in delay domain is extraordinary, so that even in a dense-scattering environment, the probability of fading is low. Since for the generation of these ultra-short pulses, no filters are required, it was considered that UWB devices are cheap to produce.

Recently, however, several drawbacks have been noted. Even though UWB transmitters irradiate very low power per bandwidth, they can potentially interfere with many systems that have frequencies assigned in the low GHz range [1]. Furthermore, multipath fading may be low, but in order to catch about half of the energy that is distributed in the entire impulse response, RAKE receivers with at least 20, but potentially many more taps must be constructed [2], [3]; for handsets, such a design is not low-cost.

We claim that both these drawbacks can be overcome if UWB is combined with a transmission scheme which is called time reversal (TR). This scheme has its origin in wide-band transmission in under-water acoustics [4], [5], [6], [7] and ultra-sound [8], [7] and has recently attracted attention of wireless communications engineers [9]. In TR, the time-reversed channel impulse response (CIR) of any transmit-receive link is taken as a prefilter at the transmitter. If such a time-reversed sequence is irradiated into the channel, its components retrace their former paths and lead to a focus of power at the intended receiver at some particular time instant. For UWB communications, this strategy has several advantages. Focusing power means that the receiver needs only very few taps to capture a significant amount of the power in the channel. Essentially, the complex taks of estimating a large number of channel taps is removed from the receiver, which may be a low-cost handset, to the transmitter. In addition, the rate of the system can be increased. Whereas with proposed pulse-position modulation schemes the time between the repetition of two pulses is chosen to be sufficiently larger than the length of the CIR [10], focusing of power means that the repetition rate can be increased. At last, the spatial focusing that comes along with TR yields lower interference with other communication systems.

In this paper, we apply TR to a single user downlink scenario of an UWB channel. In order to assess the usefulness of TR, we define a time-compression factor which measures the fraction of the energy in the non-focused components of the channel versus that in the main, focused peak. For a channel with iid complex zero mean circularly symmetric taps, 50% percent of the entire CIR's energy can be captured with a single tap receiver. In real channels, this ratio is slightly lower, which we show with the aid of experimental data from UWB measurements.

Since the scattered components are usually widely distributed over the delay axis, a receiver that wants to capture more than 50% of the signal energy in the effective CIR must use some equalization technique. We propose an TR-MMSE equalizer for this purpose. We investigate the performance of this equalizer on real channel data and show that it can operate at sampling rates which are much higher than the inverse of the length of the CIR of the channel; no ringing out of the impulse response is required.

This paper is organized as follows: in the second section, we introduce TR and define and investigate the time compression factor. Also, the signal model is described and the principles of the TR-MMSE equalizer are outlined. In the third section, we first investigate the time compression factor with the aid of real data. Then, we examine the performance of the TR-MMSE equalizer in term of bit-error-rates (BER). In particular, we vary the number of taps and the sampling rate. We conclude in Section IV.

II. Theory

A. Time Reversal

The transmitter uses the time reversed complex conjugate of the CIR as the transmit prefilter. We denote this CIR by $h(\mathbf{r_0}, \tau)$, where $\mathbf{r_0}$ is the receiver location and τ is the delay variable. Applying the complex conjugate $h^*(\mathbf{r_0}, -\tau)$ as the prefilter, the effective channel to any location $\mathbf{r}$ is thus given by the time reversed field

$$g(\mathbf{r}, \tau) \triangleq \frac{1}{\sqrt{E_H}} h^*(\mathbf{r}_0, -\tau) \otimes h(\mathbf{r}, \tau) \qquad (1)$$

where $\otimes$ denotes convolution and the factor $\frac{1}{\sqrt{E_H}}$ normalizes the transmit power with the square root of the channel's energy, $E_H = \int |h(\mathbf{r}_0, \tau)|^2 \mathrm{d}\tau$.

A convolution with a time-reversed signal is equivalent to a correlation. We see from (1) that the focusing relies on the decorrelation of CIRs in the delay and the spatial domain. In a rich scattering environment, a CIR can be considered as a random code sequence that is assigned to any transmit-receive pair. The auto- and crosscorrelation properties of this sequence are given by nature; unlike in CDMA, they come without any additional bandwidth spreading. In UWB, these sequences are particularly long. The benefits of time compression are crucial, and the shortening of the CIR reduces the complexity of equalization at the receiver.

The decorrelation of the CIRs is obviously best in a rich scattering environment. Physically, one can consider the ubiquitous locations of the scatterers to form a large virtual aperture which enables focusing even with a single antenna down to the diffraction limit. A simple but effective measure for the focusing capability of a TR channel is the delay spread-bandwidth product which roughly gives the number of taps that the CIRs has. For an initial evaluation of the benefits of TR we refer to [9].

B. Temporal Focusing

In a multipath environment, the channel's energy E_H is spread over delay. It can be decomposed into a term E_0 which describes the fraction of the energy in the direct path, and a term E_S, describing that of the multipaths. In a strong multipath environment such as given for UWB, we have the ratio $E_S/E_0 \gg 1$. If the channel is slowly time-variant, the quantities E_S, E_0, and E_H are random variables. Their mean is denoted by $\langle . \rangle$.

In TR, the CIR is compressed and a temporal focus of energy is visible in the center of the compressed CIR. In order to characterize the amount of the temporal focusing, we define the temporal compression ratio as

$$\gamma_{TR} = \langle E_S^{TR} \rangle / \langle E_0^{TR} \rangle = \frac{\langle E_H^{TR} \rangle}{\langle E_0^{TR} \rangle} - 1 \tag{2}$$

where E_0^{TR} is the energy in the main peak of the received impulse response, E_S^{TR} the one in the tails, and E_H^{TR} is the sum of the two.

We can compute γ_{TR} in terms of either the CIR $h(\tau)$ or the transfer function $H(\omega)$. From (1) we see that the transfer function $H^{TR}(\omega)$ of the time-reversed channel is the squared absolute value of that of $H(\omega)$. The discrete CIR $h^{TR}[l]$, with a total of L non-zero taps, is

$$h^{TR}[l] = \frac{1}{2\pi} \int_{-\pi}^{\pi} |H(\omega)|^2 \exp(j\omega l) \mathrm{d}\omega. \tag{3}$$

From this we compute the energy of the 0th tap of the time-reversed channel,

$$\begin{aligned} \langle E_0^{TR} \rangle &= \langle |h^{TR}[0]|^2 \rangle = \langle |\frac{1}{2\pi} \int_{-\pi}^{\pi} |H(\omega)|^2 \mathrm{d}\omega|^2 \rangle \\ &= \langle (E_S + E_0)^2 \rangle = \langle E_H^2 \rangle \end{aligned} \tag{4}$$

and the energy of the entire channel,

$$\langle E_H^{TR} \rangle = \langle \sum_l |h[l] \otimes h^*[-l]|^2 \rangle = \frac{1}{2\pi} \langle \int_{-\pi}^{\pi} |H(\omega)|^4 \mathrm{d}\omega \rangle \tag{5}$$

where the frequency domain representation on the right hand side of the equation follows from Parseval's theorem. Whether a time domain or a frequency domain representation is more desirable depends on in which domain information about the channel is available.

If we evaluate expression (5) further in time domain for L identical and independently distributed taps with equal power, we can, derive the time compression factor as

$$\gamma^{TR} = \frac{\beta_4 + 2(L-1)\beta_2^2}{\beta_4 + (L-1)\beta_2^2} - 1. \tag{6}$$

Here, β_2 and β_4 denote the second and the fourth moment of the amplitude in each tap, respectively. For $L = 1$, one has $\gamma^{TR} = 0$; with increasing L it converges to 1. Hence, in the time-reversal channel, the ratio of the energy of the zeroth tap to the sum of the energy of all the other taps converges to a fixed value.

If $h[l]$ is a complex Gaussian random variable with mean 0 and variance $\langle E_0 + E_S \rangle = \langle E_H \rangle$, we have $\beta_2 = \langle E_H \rangle$ and $\beta_4 = 2\langle E_H \rangle^2$. Hence,

$$\gamma_{TR} = \frac{2L\langle E_H \rangle^2}{2\langle E_H \rangle^2 + (L-1)\langle E_H \rangle^2} - 1 = \frac{2}{1 + \frac{1}{L}} - 1. \tag{7}$$

For large L, the power in the tails of the impulse response becomes about equal the power in the peak. Hence, even though ISI can be significantly suppressed, any system without equalization operates at best at 0 dB signal to ISI plus noise ratio. For small L, the compression works in the mean better than for a large one, even though the difference quickly levels out. But the probability that a channel realization occurs that does not focus at all (i.e., all channel taps are real and have the same magnitude) is much larger than for long sequences.

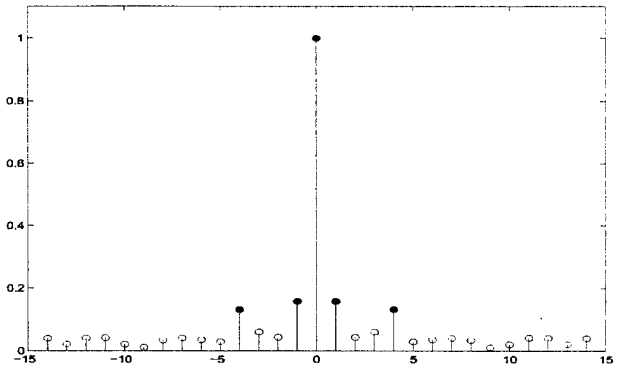

Fig. 1. Schematic of TR impulse h_{TR} and truncated TR CIR h_{TR}^s. In this toy example $L = 29$, $L_s = 9$ and the number of effective taps (marked as filled circles) is 5.

C. Signal Model and TR-MMSE Equalizer

The transmitter modulates symbols s_k using a pulse shaping filter $\phi(\tau)$ of bandwidth $B = 1/T_s$. It then performs TR on the pulse stream. Thus:

$$x(t) = \sum_k s_k \phi(t - kMT_s) \otimes \tilde{h}^*(-t) \tag{8}$$

where $\tilde{h}(\tau)$ is the (infinite bandwidth) CIR. After matched filtering the received signal can be written as:

$$y(t) = \sum_k s_k \phi(t - kMT_s) \otimes \tilde{h}^*(-t) \otimes \tilde{h}(t) \otimes \phi^*(-t) + n(t) \tag{9}$$

The receiver then samples $y(t)$ at lMT_s:

$$y[l] = y(lMT_s) = \sum_k s_k h_{TR}[l-k] + n[l], \tag{10}$$

where $h_{TR}(t) = h(t) \otimes h^*(-t)$, $h(t) = \tilde{h}(t) \otimes \phi(t)$, and $h_{TR}[k] = h_{TR}(kMT_s)$. The sampled received signal is thus the convolution of the symbols with a downsampled-by-M version of $h_{TR}(.)$.

Due to the temporal focusing described above the equalizer at the receiver does not have to use the quite long (time-reversed) CIR. Instead the equalizer uses a "shortened" TR CIR by keeping only a few taps which capture most of the energy of h_{TR} and still achieve very good performance. More precisely, we construct a shortened TR CIR h_{TR}^s of length L_s as illustrated in Fig. 1 by defining

$$h_{TR}^s[l] := \begin{cases} h_{TR}[l] & \text{if } |h_{TR}[l]| \geq \delta, \\ 0 & \text{else,} \end{cases} \tag{11}$$

for $|l| \leq L_s/2$ and $L_s = \max\{l : |h_{TR}[l]| \geq \delta\}$. Here δ is an a priori chosen tolerance level that depends on the target SNR. For convenience we will rename the indexing of h_{TR}^s such that $h_{TR}^s = [h_{TR}^s[0], \ldots, h_{TR}^s[L_s - 1]]^*$.

The symbols are transmitted one block at a time with a guard period of length L_s. The output of the channel is:

$$y[m] = (x \otimes h_{TR})[m] + n_R[m]$$

Here $x[m]$ is the input signal $m = 0, \ldots, N-1$ and $y[m]$ is the output signal $m = 0, \ldots, N+L-2$. In matrix notation this can be written as Toeplitz-type system

$$\mathbf{y} = \mathbf{H}_{TR}\mathbf{x} + \mathbf{n}_R$$

where $\mathbf{y} = [y[0] \ldots y[N+L-2]]^T$ and $\mathbf{x} = [x[0] \ldots x[N-1]]^T$. Using h^s_{TR} instead of h_{TR} for the MMSE equalizer we replace $\mathbf{H}_{TR}$ by the matrix $\mathbf{H}^s_{TR}$ of size $(N+L_s-1) \times N$ given by

$$\mathbf{H}^s_{TR} = \begin{bmatrix} h^s_{TR}[0] & 0 & \ldots & 0 \\ \vdots & & & \\ h^s_{TR}[L_s-1] & & \ddots & \vdots \\ 0 & & & 0 \\ & \ddots & & h^s_{TR}[0] \\ \vdots & & & \vdots \\ 0 & \ldots & 0 & h^s_{TR}[L_s-1] \end{bmatrix},$$

and the matrix equation for the MMSE estimator becomes

$$\hat{\mathbf{x}} = \left((\mathbf{H}^s_{TR})^* \mathbf{H}^s_{TR} + \frac{1}{SNR_{RX}} \mathbf{I} \right)^{-1} (\mathbf{H}^s_{TR})^* \mathbf{y}.$$

Assuming the transmitted symbols are from a BPSK alphabet, we can now decode $\hat{\mathbf{x}}$ by looking at the sign of each element.

We note that $\mathbf{H}^s_{TR}$ is a sparse Toeplitz matrix, thus $\hat{\mathbf{x}}$ can be computed efficiently by combining sparse matrix techniques with fast Toeplitz solvers [11].

III. Simulations

A. Measurement Data and Temporal Focusing

Measurements were conducted with a network analyzer by Intel Corp. at off-peak hours to ensure channel stationarity. The environment is an office space (40m × 60m) with many cubicles; measurements were conducted at several locations. They span a bandwidth of 2-8 GHz with 3.75 MHz frequency resolution. Antennas are vertically polarized. The measurements are corrected to compensate for the system components (including cable, gain stages, and antennas). The height of the transmit antenna is about 2.5m and that of the receive antenna is 1m above the floor. As a sample result, Fig. 2 shows the CIR (above) and the time-reversed CIR (below). The compression is clearly visible. Still, this figure is not suitable to tell the ratio between the power in the peak of the time-reversed impulse response and that in the tails. In order to demonstrate this ratio, we plotted in Fig. 3 the time compression ratio γ_{TR} for a CIR length between 1 and 500 taps, where the entire length of the CIR is fixed at 1/3.75MHz. The curve was actually computed in frequency domain; in order to suppress fluctuations due to the randomness of the samples, a sliding window was implemented, so that γ_{TR} was actually averaged over all available frequency samples.

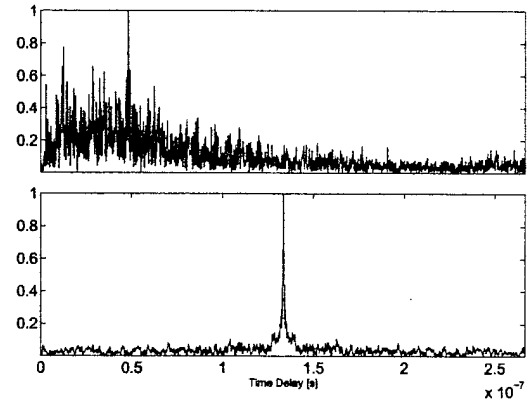

Fig. 2. Impulse Response of the channel (above) and of the time-reversed channel (below)

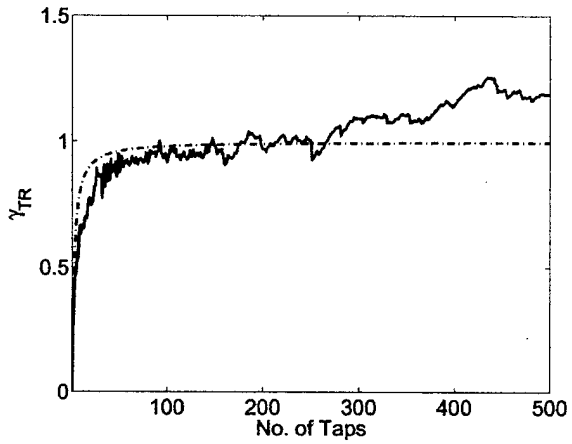

Fig. 3. In the TR channel, the ratio between the eneregy in the main tap and the energy in the tail of the CIR converges for independent taps to a fixed ratio.

For a small number of taps, the curve coincides very well with the theoretical one. At about 200 taps, the maximum theoretical value of 1 is exceeded; beyond that, correlation between the taps starts to play a role and the power in the tails of the CIR will be stronger than that in the main peak.

B. Performance of the Equalizer

We used the single channel realization whose magnitude response at full bandwidth, B, is shown in Fig. 2. Three cases were considered. Case I has $M = 8$ (see Eqn. 10) and bandwidth B. Case II has $M = 4$ and bandwidth $B/2$. Finally case III has $M = 2$ and bandwidth $B/4$. The constellation was BPSK and no channel coding was used. Thus all the scenarios have the same data rate and all channels have 250 taps. Fig. 4 shows the bit error rate (BER) curves for these scenarios when the receiver only estimates the 20 strongest taps. When $M = 2$ the curve floors very rapidly since not a very significant portion of the energy of the CIR is captured by the largest 20 taps. When $M = 4$, the ISI energy is due only to every fourth tap of the TR channel. Thus more of the energy

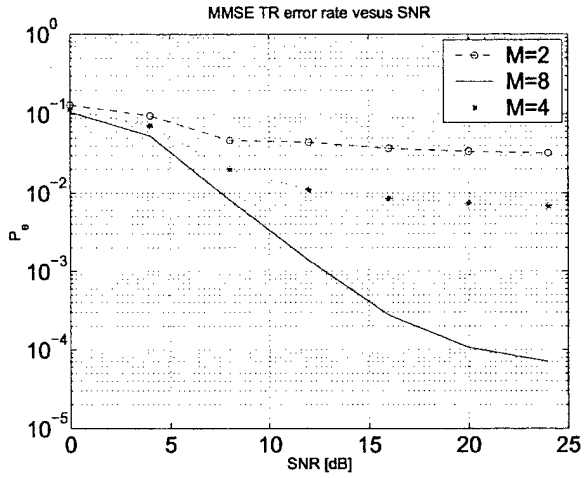

Fig. 4. BER vs SNR when the receiver only estimates the 20 largest taps of the channel. Bandwidth expansion factor of 8 (solid line), 4 (dotted line), and 2 (dashed line)

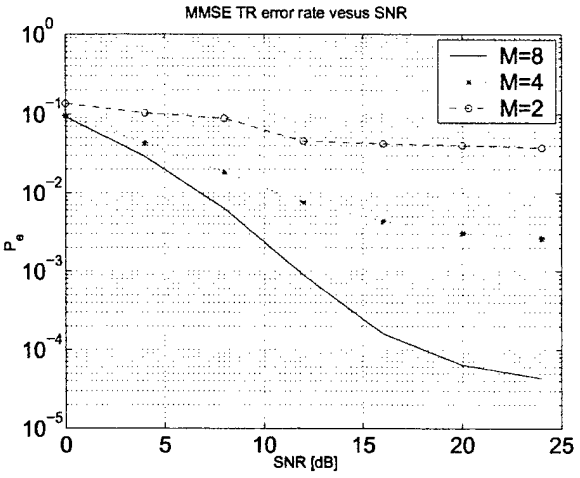

Fig. 6. BER vs SNR when the receiver only estimates 20 largest taps of the channel - another channel realization. Bandwidth expansion factor of 8 (solid line), 4 (dotted line) and 2 (dashed line).

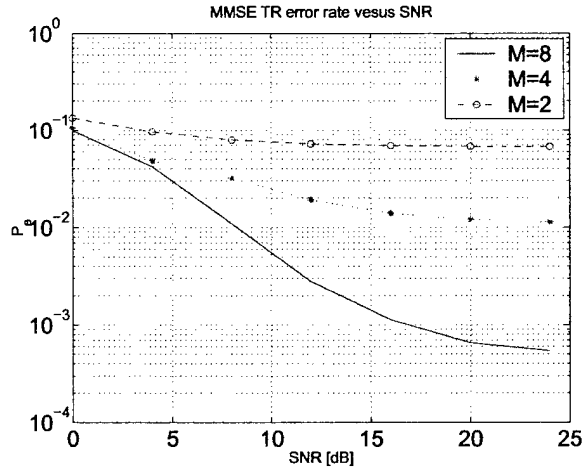

Fig. 5. BER vs SNR when the receiver only estimates the 10 largest taps of the channel. Bandwidth expansion factor of 8 (solid line), 4 (dotted line), and 2 (dashed line)

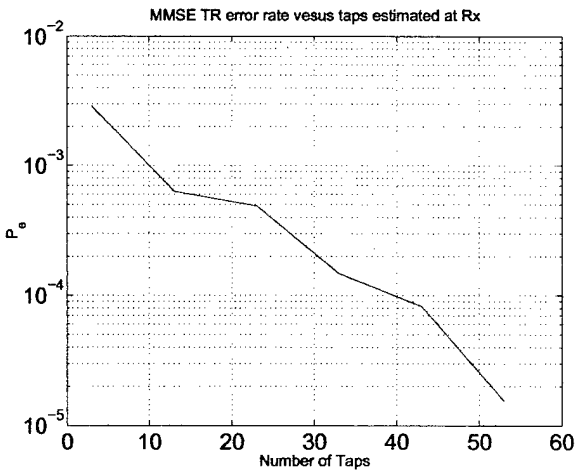

Fig. 7. BER vs number of strongest taps estimated at the receiver. SNR = 15 dB

of the effective CIR is captured by the strongest 20 taps. This effect improves significantly in the case where $M = 8$. Note that the case $M = 8$ uses more bandwidth. However, the BER floors at a reasonable SNR of 15 dB for UWB. Fig. 5 shows the BER curves for the same three cases but when the receiver estimates only 10 strongest taps of the CIR. In this scenario the error flooring occurs earlier for all the cases. However, the complexity of the receiver is significantly reduced.

Fig. 6 plots the BER for a different CIR. Here the receiver estimates the largest 20 taps of the CIR. Comparison between this figure and Fig. 4 shows that the BER performance is very similar for these two channel realizations. This is due to the large diversity available in this ultra-wideband channel.

Fig. 7 shows the BER vs number of strongest CIR taps that the receiver estimates for equalization at 15 dB SNR. This plot shows that the BER reduces approximately exponentially with increasing number of taps. Fig. 8 shows the BER vs number of strongest CIR taps that the receiver estimates at 15 dB SNR when the transmitter does not use TR. Figs. 7 and 8 demonstrate the temporal focusing ability of TR. The receiver requires to estimate much less taps with TR than without it in order to achieve the same BER performance.

Note that the plots are for the strongest taps. These taps may not be next to one another. There may be zeros between any two consecutive strongest taps. Thus the total length in samples of the estimated channel is in general larger than the number of strongest taps estimated. However, the complexity of equalization is approximately the same as if the length of the estimated channel is equal to the strongest number of taps estimated.

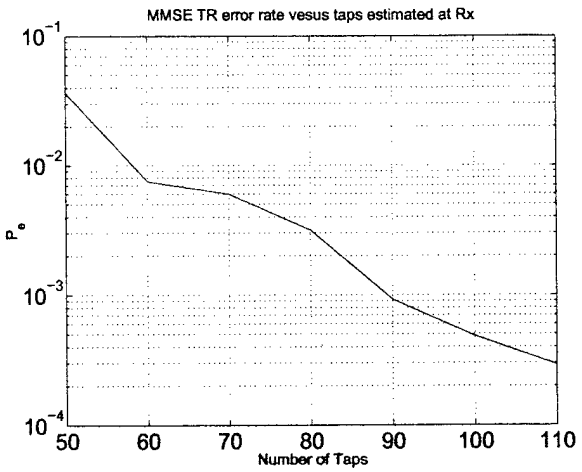

Fig. 8. BER vs number of strongest taps estimated at the receiver with regular transmission. SNR = 15 dB

IV. Conclusion

Time reversal significantly reduces the number of taps that the receiver needs to estimate in order to achieve a certain target BER. If the CIR has iid complex Gaussian taps the ratio of signal to ISI power approaches unity as the length of the CIR increases without bound. We show that this ratio is very close to unity when the CIR is more than about 10 taps long.

In order to mitigate the ISI one can fix the bandwidth and increase symbol spacing by an integer factor of M. The larger M, the less taps of the CIR the receiver needs to estimate in order to attain a reasonable BER. However, larger M means more wasted bandwidth. With no channel coding and by only estimating the 20 strongest taps out of approximately 250 channel taps, the receiver can reach 10^{-3} BER at around 12 dB SNR with MMSE equalization and $M = 8$. In order to achieve such a performance without TR, the receiver needs to estimate almost all the taps of the CIR.

References

[1] M. Z. Win and R. A. Scholtz, "Impulse radio: How it works," *IEEE Commun. Lett.*, vol. 2, no. 2, pp. 36–38, Feb. 1998.

[2] ——, "On the energy capture of ultrawide bandwidth signals in dense multipath environments," *IEEE Commun. Lett.*, vol. 2, no. 9, pp. 245–247, Sept. 1998.

[3] ——, "Characterization of ultra-wide bandwidth wireless indoor channels: A communication-theoretic view," *IEEE J. Select. Areas Commun.*, vol. 20, no. 9, pp. 1613–1627, Dec. 2002.

[4] D. Rouseff *et al.*, "Underwater acoustic communication by passive-phase conjugation: Theory and experimental results," *IEEE Journal of Oceanic Engineering*, vol. 26, pp. 821–831, 2001.

[5] M. G. Heinemann, A. Larazza, and K. B. Smith, "Acoustic communications in an enclosure using single-channel time-reversal acoustics," *Appl. Phys. Lett.*, vol. 80, pp. 694–696, 2002.

[6] G. F. Edelmann *et al.*, "An initial demonstration of underwater acoustic communications using time reversal," *IEEE Journal of Oceanic Engineering*, vol. 27, pp. 602–609, 2002.

[7] A. Derode *et al.*, "Taking advantage of multiple scattering to communicate with time-reversal antennas," *Phys. Rev. Letters*, vol. 90, 2003.

[8] A. Derode, P. Roux, and M. Fink, "Robust acoustic time reversal with high-order multiple scattering," *Phys. Rev. Letters*, vol. 75, pp. 4206–4209, 1995.

[9] S. M. Emami, J. Hansen, A. D. Kim, G. Papanicolaou, A. J. Paulraj, D. Cheung, and C. Prettie, "Predicted time reversal performance in wireless communications using channel measurements," *IEEE Communications Letters*, 2004, accepted for publication.

[10] J. D. Choi and W. E. Stark, "Performance of ultra-wideband communications with suboptimal receivers in multipath channels," *IEEE J. Select. Areas Commun.*, vol. 20, no. 9, pp. 1754–1766, Dec. 2002.

[11] G. Golub and C. van Loan, *Matrix Computations*, 3rd ed. Baltimore: Johns Hopkins, 1996.

Matched Filtering with Rate Back-off for Low Complexity Communications in Very Large Delay Spread Channels

Majid Emami[1], *Mai Vu*[1], *Jan Hansen*[1], *Arogyaswami J. Paulraj*[1], *and George Papanicolaou*[2]

[1] Information Systems Laboratory, Stanford University, Stanford, CA 94305, USA.

Fax: 650-723-8473, Email: {memami, mhv, jchansen, apaulraj}@stanford.edu

[2] Department of Mathematics, Stanford University, Stanford, CA 94305, USA. Email: papanicolaou@stanford.edu

EXTENDED ABSTRACT

We study the possibility to transmit data over channels with large delay spreads under the constraint of a very simple receiver which has only one tap. Such a scheme is of interest when a cost-efficient way to transmit potentially large data rates is sought. We investigate the performance of the optimal prefilter for this scheme, and compare it to a simplified, so-called time-reversal, prefilter which has very low complexity. Time reversal filters have in connection with wireless transmission over large bandwidths their origin in underwater acoustics and ultrasound [1]. Their application to wireless communications was recently demonstrated on UWB data [2]. At low SNR, the optimal prefilter and the TR prefilter are equivalent. At high SNR, the time reversal prefilter achieves a performance that is independent from the delay spread of the channel and hence the same for any bandwidth.

In this contribution we derive analytically the performance of the discussed system. We discuss the impact of multiple transmit antennas and of a transmission scheme that uses rate back-off, i.e., it transmits at a rate lower than the inverse of the bandwidth. If bandwidth is abundant, such as it is the case in Ultra-wideband communications [3], our proposed scheme can achieve a reliable quality of service at high data rates with a single tap receiver. We mention that our setup corresponds to the downlink of an access point to a handheld. In principle, our analysis holds equivalently for a simple transmitter with a receive equalizer with a large number of taps.

A. Prefiltering for Long Delay Spread Channels

A block diagram of the system under study is given in Fig. 1. The transmit symbols x are fed into equalizers g_i and then transmitted through the channels described by their channel impulse responses (CIRs) h_i, $i = 1, \ldots, M_T$, and M_T is the number of transmit antennas. The noise is denoted by n, and the receiver has a single tap whose gain is denoted by β. Since with very large delay spread the transmit prefilter is not likely to eliminate inter signal interference (ISI) completely, we allow that the system does not transmit at full rate (inverse bandwidth), but at a integer fraction of this rate, which we call D. The input-output

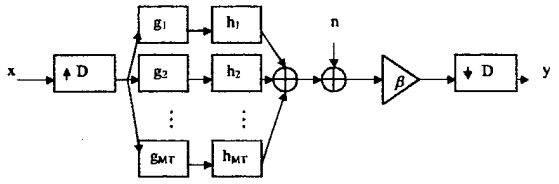

Fig. 1. A block diagram of a MISO system with a preequalizer at the transmitter and a single tap receiver.

relation of this system can be written as

$$y^{[D]}[k] = \beta \sum_{i=1}^{M_T} \sum_{l} (h_i * g_i)[Dl]x[k-l] + \beta n[k] \quad (1)$$

where $y^{[D]}[k]$ is the output symbol at time k. The rate back-off factor $D = 1, \ldots, L$ is equivalent to upsampling the signal before transmission by a factor of D, and L is the channel length.

We derive the optimal prefilter solving the minimization problem

$$\begin{aligned} \hat{\mathbf{g}}_{\beta,N} &= \text{argmax}_{\mathbf{g},\beta} E[\| \mathbf{x}_k \beta \mathbf{H}\mathbf{g} + \beta n[k] - x[k-\Delta] \|^2] \\ &\text{s.t. } E \| \mathbf{g}^H \mathbf{g} \| = 1. \end{aligned} \quad (2)$$

The product $\mathbf{Hg}$ is the convolution of the prefilter and the channel, the latter stacked into a toeplitz matrix, and N is the length of the filter. The vector $\mathbf{g}$ is given by

$$\mathbf{g} = [\mathbf{g}[0]^T \quad \ldots \quad \mathbf{g}[N-1]^T]^T \quad (3)$$

and

$$\mathbf{g}[l] = [g_1[l] \quad \ldots \quad g_{M_T}[l]]^T \quad l = 0, \ldots, N-1. \quad (4)$$

Δ is the delay of the equalizer and is approximately $\frac{N+L}{2}$. The difference between this formulation and the one where the equalizer is placed at the receiver is the transmit power constraint. The above problem is convex in $\mathbf{g}$ and β and can be solved analytically using the method of Lagrange multipliers:

$$\hat{\mathbf{g}}_{\beta,N} = \frac{1}{\beta} \left(\mathbf{H}^H \mathbf{H} + \frac{\sigma^2}{P} \mathbf{I} \right)^{-1} \mathbf{H}^H \hat{\mathbf{e}}_\Delta \quad (5)$$

$$\beta^2 = \hat{\mathbf{e}}_\Delta^T \mathbf{H} \left(\mathbf{H}^H \mathbf{H} + \frac{\sigma^2}{P} \mathbf{I} \right)^{-2} \mathbf{H}^H \hat{\mathbf{e}}_\Delta \quad (6)$$

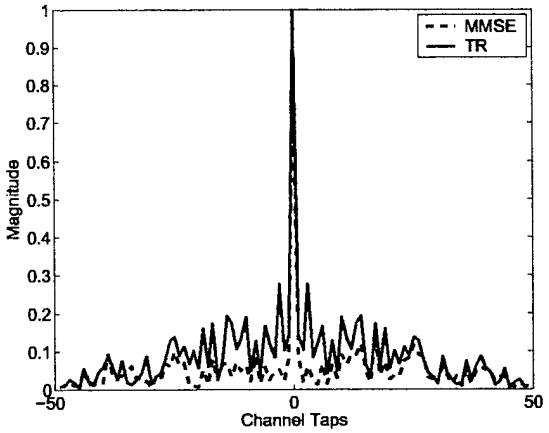

Fig. 2. The effective channel as generated by TR (dashed line) and the MMSE filter (cont. line)

Eq. (5) defines a filter with an MMSE-type solution with a finite number of taps. We notice that the optimized value for β bascially ensures that the power constraint of the filter is valid. In the transmit-receiver chain of Fig. 1, β has no effect on the SNR at the receiver; it ensures, however, that the transmitter can take into account the SNR to optimize the preequalizer.

We introduce a simplified filter which we call TR-prefilter and which basically is a matched prefilter; it follows from the optimal filter (5) for low SNR,

$$\begin{aligned} \mathbf{g}_{TR} &= \lim_{SNR \to 0} \mathbf{g} = \mathbf{h}^* \\ & s.t. \parallel \mathbf{h} \parallel = 1, \end{aligned} \tag{7}$$

or

$$g_{TR,i}[k] = \sqrt{\gamma} h_i^*[-k],$$

with $\gamma = \left(\sum_{i=1}^{M_T} \sum_{l=1}^{L-1} |h_i[l]|^2 \right)^{-1}$, i.e., the filter equals the time-reversed CIR of the channel, and the receiver receives the autocorrelation function of the channel. The power in its central peak is maximized, but the ISI suppression is worse.

The CIR of a pre-equalized channel with originally 50 taps and constant power delay profile is shown in Fig. 2; for the computation of the MMSE filter, $\rho = P_{Tx}/\sigma^2 = 5$ dB was assumed. The dashed line is obtained from the MMSE filter, the continuous one from the TR prefilter. We see that the prefilters compress the CIRs significantly around a strong peak. The ISI of the impulse response obtained with TR is higher than that of the MMSE filter, but its peak is slightly higher, too. For a large number of taps, the peak is essentially non-fading which yields reliable system performance.

B. Performance Evaluation of the TR filter

For performance evaluation, we denote by P_0 and $Q^{[D]}$ the instant useful power and the ISI power, respectively, and define the effective SNR ρ_{eff} as

$$\rho_{eff,D} = \frac{P_{Tx} E[P_0]}{P_{Tx} E[Q^{[D]}] + \sigma^2} = \frac{E[P_0]}{E[Q^{[D]}] + \frac{1}{\rho}}. \tag{8}$$

We furthermore define the matched-filter bound SNR ρ_{MFB} as

$$\rho_{MFB} = \frac{P_{Tx} E[\sum_{i=1}^{M_T} \sum_l |h_i[l]|^2]}{\sigma^2}. \tag{9}$$

Combining (8) and (9) we have that the effective SNR of a TR communication system with M_T transmit antennas and a rate-back off of D is

$$\rho_{eff,D} = \rho_{MFB} \frac{1}{1 + \rho_{MFB} \frac{E[Q_{TR}^{[D]}]}{E[P_{TR}]}}. \tag{10}$$

In our paper we will present a formula for the ratio of the useful power against the ISI power, $E[P_{TR}]/E[Q_{TR}^{[D]}]$ for a channel with exponentially decaying power delay profile and delay spread σ_τ. Using this result, we derive the following limiting cases:

$$\rho_{eff,D} = \rho_{MFB} \quad \text{for } \sigma_\tau \longrightarrow 0 \tag{11}$$

$$\rho_{eff,D} = \frac{D M_T \rho_{MFB}}{\rho_{MFB} + D M_T} \quad \text{for } \sigma_\tau \longrightarrow \infty \tag{12}$$

Eq. (11) tells that a TR system is lossless should the delay spread of the channel be very small. Eq. (12) can be split into a low-SNR and a high-SNR regime as

$$\rho_{eff,D} = \rho_{MFB} \quad \text{for } \rho_{MFB} \text{ low, } \sigma_\tau \text{ large} \tag{13}$$

$$\rho_{eff,D} = D M_T \quad \text{for } \rho_{MFB}, \sigma_\tau \text{ large.} \tag{14}$$

Eq. (13) shows that TR is optimal at low SNR; this behavior is expected for a transmit matched filter. Numerical results presented in the final paper will show, however, that the low-SNR region ends at about 0 dB which not sufficient for reliable communications. Eq. (14) demonstrates that in an environment with a large delay spread σ_τ, the performance of a TR system at high input SNR saturates at a value independent from the delay spread of the channel. The performance increases with 3 dB per added transmit antenna, and with another 3 dB for each rate-back off of a factor 2 from the maximum available bandwidth. We will also include simulations that show that the central tap is non-fading.

If bandwidth is abundant, we can hence design a communication system with a very simple receiver that has only one tap and does not need to perform channel estimation. This tap is non-fading and the effective SNR is not a function of the bandwidth of the system. Varation of transmission rate or using some particular number of transmit antennas guarantees any reasonable quality of service. In our final paper we will discuss the derivations and results presented here more thoroughly, give some numerical examples which highlight some of the analytical results, and point out future applications of the investigated system.

REFERENCES

[1] A. Derode, P. Roux, and M. Fink, "Robust acoustic time reversal with high-order multiple scattering," *Phys. Rev. Letters*, vol. 75, pp. 4206–4209, 1995.

[2] S. M. Emami, J. Hansen, A. D. Kim, G. Papanicolaou, A. J. Paulraj, D. Cheung, and C. Prettie, "Predicted time reversal performance in wireless communications using channel measurements," *IEEE Communications Letters*, 2004, accepted for publication.

[3] D. Porcino and W. Hirt, "Ultra-wideband radio technology: Potential and challenges ahead," *IEEE Communications Magazine*, pp. 66–74, July 2003.

Time Reversal Techniques for Broadband Wireless Communication Systems

Claude Oestges*, Jan Hansen†, Seyed M. Emami†, Arnold D. Kim‡, George Papanicolaou§, and Arogyaswami J. Paulraj†

*Microwave Laboratory, Université catholique de Louvain, Louvain-la-Neuve, Belgium
†Information Systems Laboratory, Stanford University, Stanford, CA
‡School of Natural Sciences, University of California, Merced, CA
§Department of Mathematics, Stanford University, Stanford, CA

Abstract—**Channels with large delay spreads, which typically arise when large bandwidths are used, are considered as disadvantageous for wireless communications. However, despite their challenges, these channels also offer opportunities. The application of time reversal techniques may be one possibility to exploit these advantages and to make communications in channels with large delay spreads more feasible. This paper describes advantages and draw backs of time reversal techniques in broadband wireless communications, and outlines concepts, goals and potential improvements. The properties of time reversal in various simulated and measured wireless channels are demonstrated, and system design is discussed.**

I. Introduction

While there is little doubt that future communication systems will have to accomodate larger data rates, the natural solution consisting of increasing the bandwidth brings a number of open challenges. In this matter, time reversal (TR) techniques could play a role in the design of broadband wireless communications. In TR, channel state information (CSI) at one or possibly more transmit antennas is used to precode transmitted symbols with the time reversed version of their respective channel impulse responses (CIRs). These "time reversed" waves propagate in the channel, retrace their former paths and eventually lead to a focus of power in space and time at the receiver [1]–[3]. In rich scattering media, this space-time compression can be very strong, and at the focal point, the effective channel obtained through TR is hardened.

Spatial focusing [4] means that the spatial profile of the power peaks at the intended receiver and decays rapidly away from the receiver. Temporal focusing means that the CIR at the receiver has a very short effective length. Channel hardening is the phenomenon of tightening of the distribution function of the effective CIR's power.

Using TR for wireless communications in channels with large delay spreads presents therefore three merits.

- The temporal focusing compresses the channel's energy into one single peak with very low sidelobes. The task of equalizing the channel is hence significantly simplified.
- The spatial focusing can result in much lower intercept probability and co-channel interference in a multi-cell system. By selectively focusing the energy in both space and time at a target point, TR ensures that intercept receivers will have difficulty detecting or decoding the intended signal.
- Through the channel hardening, TR provides high diversity gain. The statistics of the time reversed channel are different from the actual channel. Specifically the time reversed channel has a much smaller variance than the physical channel itself.

Time reversal is well known in acoustics and has lead to remarkable applications in underwater sound [5]–[13] and ultrasound [14]–[16]. The extension of TR techniques to wireless communications has yet to be precisely investigated, although the idea of exploiting scattering has recently been proposed in [17]–[20]. From a communication engineer's viewpoint, TR shifts the system's matched filter from the receiver side into the channel. The complexity of the transmitter increases; the receiver captures a preequalized CIR which is, in the case of large delay spread channels, much simpler to equalize than the original one. Research on TR touches a number of different research areas. Seen as a preequalizer, TR is known as a transmit matched filter [21] or pre-rake [22] which has been studied in connection with CDMA but not at very large delay spreads, where spatial and temporal focusing comes into effect. TR has to be compared to optimal schemes (e.g. [23], [24]). Complexity will become a major issue since delay spreads of 100 or more taps can make many known optimal schemes infeasable. The spectral efficiency is also of great interest. TR does not use the capacity achieving power allocation [25], but in fading channels, an increased bandwidth yields channel hardening which could increase outage capacity. Finally, many practical issues need to be addressed. At which bandwidth does it become advantageous to precode transmitted messages in order to shorten the channel, and which precoding method should be applied? At which size of a network does it become useful to shift complexity from several receivers to one centralized transmitter? We believe that the recent interest in transmission over very large bandwidths such as provided by the standard IEEE 802.15 [26] is a good incentive to rethink many of the long known methods that were invented to deal with channels of low and moderate delay spread. We propose TR as a suitable starting point for these investigations, as it clearly points out the potential gains that high-delay spread

channels may offer despite their draw backs.

Here, we shall present an initial study of TR applied to radio wireless systems. In Section II, we briefly introduce TR, together with the formalism used in this paper. In Section III, we compare the rate of a TR system to one that uses waterfilling and we simulate the cumulative distribution function of the rate of such a system in a fading channel. Section IV deals with the characterization of time-reversed random fields in wireless channels. To this end, we first define suitable metrics in order to characterize temporal and spatial focusing. Then we present measured results of TR space-time focusing in an indoor Ultra Wide Band (UWB) radio channel in the 2-8 GHz band [28]. To provide more insight in the space-time focusing results, we finally perform simulations for broadband systems (bandwidth up to 100 MHz) using two very different channel models at 2.5 GHz [27].

In Section V, we investigate the applicability of TR to wireless data transmissions. We examine how TR performs compared to optimized linear precoding, and we compute bit error rates of both a TR and an optimized system [29]. We describe in Section VI how commercially available MIMO channel sounders can be converted into sounders that can be used for real-world TR-channel measurements, and we finally conclude in Section VII.

II. Time Reversal Formulation

Consider a transmission between transmit point $\mathbf{P}$ and receive point $\mathbf{Q}$. The CIR is denoted as $h(\tau, \mathbf{P} \rightarrow \mathbf{Q})$. It is important to note that the usual symmetry properties imply that $h(\tau, \mathbf{P} \rightarrow \mathbf{Q}) = h(\tau, \mathbf{Q} \rightarrow \mathbf{P})$.

The so-called CIR is actually the convolution of the infinite-bandwidth physical channel response and the filter impulse response of bandwidth B, e.g. a Nyquist filter with given roll-off factor.

Depending on the scattering channel and the bandwidth, the CIR results in a temporal spreading of the initial pulse. Scatterers indeed create multipath mechanisms which, in turn, cause echoes to arrive at the receiver with different delays. However, the resolvability of the different delays depends upon the ratio of the inverse of the bandwidth to the physical channel spread (i.e. the interval between successive delays). The smaller $1/B$ is relative to the channel delay spread, the larger is the number of resolved paths. As an important conclusion of the above discussion, it can be expected that the $B \times \tau_{\text{RMS}}$ product will play a significant role in TR focusing results.

Using the proposed formalism, the received signal at any point $\mathbf{R}$ for a pulse emitted from $\mathbf{R}_0$ is $h(\tau, \mathbf{R}_0 \rightarrow \mathbf{R})$. At a particular point $\mathbf{T}$, which we define as the transponder, $h(\tau, \mathbf{R}_0 \rightarrow \mathbf{T})$ is captured. If the transponder sends back the time reversed version of the captured signal, i.e. $h(-\tau, \mathbf{R}_0 \rightarrow \mathbf{T})$, then at any point $\mathbf{R}$, the received signal can be expressed as

$$s(\tau, \mathbf{R}) = h(\tau, \mathbf{T} \rightarrow \mathbf{R}) \star h(-\tau, \mathbf{R}_0 \rightarrow \mathbf{T}) \qquad (1)$$

where $\star$ denotes the convolution product. Note that (1) assumes a perfect estimation of $h(\tau, \mathbf{R}_0 \rightarrow \mathbf{T})$. In practical settings, noise and interference considerations will cause this estimation to be biased. It should also be remembered that $s(\tau, \mathbf{R})$ is related to the bandwidth B.

From now on, we define the point $\mathbf{R} = \mathbf{R}_0$ as the focal, the target point or simply the receiver. Furthermore, when there is no ambiguity about the transmitter position, we also drop the symbol $\mathbf{T}$ and the arrow in the notation of the CIR.

Based on (1) and on the symmetry properties mentioned above, the signal received at $\mathbf{R}_0$ is

$$s(\tau, \mathbf{R}_0) = h(\tau, \mathbf{R}_0) \star h(-\tau, \mathbf{R}_0) \qquad (2)$$

As a consequence of (2), the time reversal operation causes the received signal at $\mathbf{R}_0$ to be focused in both time and space through constructive interference, meaning that all multipath signals add coherently at $\mathbf{R}_0$, and incoherently elsewhere.

Models usually compute the channel transfer function $H(\omega, \mathbf{R}_0)$ over the system bandwidth (where ω is the angular frequency). It is the Fourier transform of $h(\tau, \mathbf{R}_0)$. Relationships (1) and (2) are easily written in the frequency domain, since the time reversal operation corresponds to a complex conjugation in frequency (denoted by the superscript *):

$$S(\omega, \mathbf{R}_0) = H(\omega, \mathbf{R}_0) H^*(\omega, \mathbf{R}_0) \qquad (3)$$

According to (3), we observe that the time reversal operation is equivalent to a perfect channel matching, i.e., the channel acts as the system's matched filter. According to (2), we see that $s(\tau, \mathbf{R}_0)$ is the autocorrelation function of the channel, so that there is a second interpretation for TR. We may consider the CIR as a randomly generated code sequence which is given by nature. Then, a TR communication system operates similar to a broadcasting CDMA system with a pre-RAKE [22]. But the code sequence is not a spreading sequence in the sense that it spreads transmission bandwidth without increasing information rate for each single user. In TR, the fully spread bandwidth can be used for transmission to each user. However, since the sequence does not have carefully designed correlation properties but is at best random, the TR system cannot erase intersignal interference (ISI) and multiuser interference completely.

III. Capacity and Outage in TR Schemes

We compare in this section the rate of a TR system to one that uses waterfilling and simulate the cumulative distribution functions of the rates of these systems in a fading channel. TR enforces a particular power allocation scheme, $P(\omega) = |H(\omega)|^2$, which is in general not capacity achieving. The power allocation strategy inherent to TR is to enhance the strong components of the channel, and to weaken those which are less strong. At low SNR, this strategy is related to waterfilling, so that we can expect a close-to-optimal performance. At high SNR, where a constant power allocation scheme is optimal, TR is not. We demonstrate this behavior in Fig. 1 in which the mean rate of a TR communication system that operates in a channel with 50 i.i.d. Gaussian distributed taps is depicted (dashed line). The rate equals at low SNR the capacity of the channel (continuous line), and deviates more and more at higher SNR. Also for comparison, the capacity of the AWGN channel is shown. It is largest in this picture since all curves are normalized to a bandwidth of 1 Hz [25].

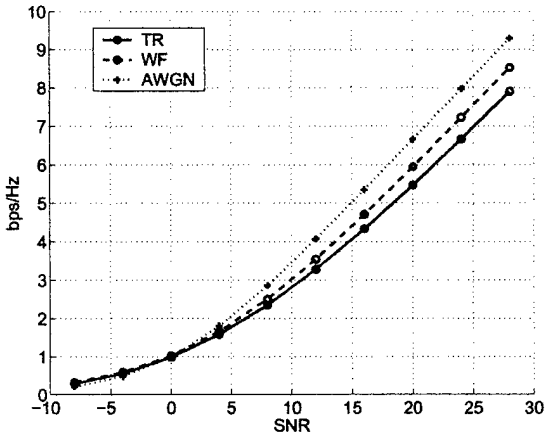

Fig. 1. The average rate of a TR communication system reaches at low SNR the capacity of the frequency selective channel.

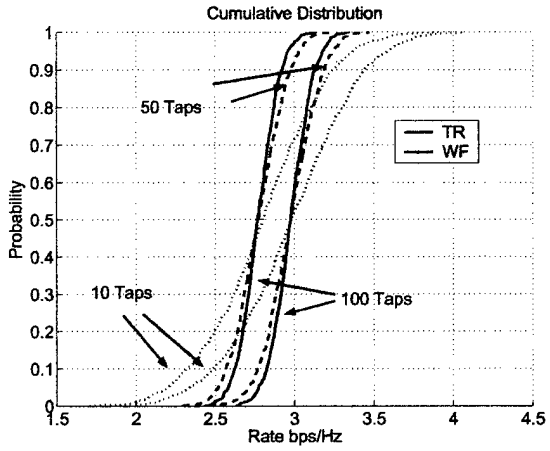

Fig. 2. In channels with a larger number of taps, the outage probability decreases.

In fading channels, outage capacity can be more relevant that ergodic capacity. The cumulative distribution function (cdf) of the rate of a TR system at 10 dB SNR in channels with 10, 50, and 100 i.i.d. Rayleigh taps is shown in Fig. 2. The cdf of the TR system is shown as the blue curves, those of a scheme that uses water filling in black. The rate of the TR system has for a particular number of taps a cdf which is very similar to that of the optimal scheme but shifted by a fixed amount of less than a quarter bps/Hz to the left. A TR system in a channel with 50 taps has at an outage probability of 20% about the same rate as an optimally precoded system that uses water filling in a channel with 10 taps. The increase from 50 to 100 taps does not improve the rate at this outage probability much.

IV. Time Reversal Channel Characterization

A. Characterization Metrics

The space-time received signal $s(\tau, \mathbf{R})$ is converted into performance metrics by considering

- the energy of $s(\tau, \mathbf{R})$ at any point $\mathbf{R}$ in space, at a given time τ_0, i.e.

$$\eta_D(\mathbf{R}) = |s(\tau_0, \mathbf{R})|^2 \tag{4}$$

  with τ_0 such that $|s(\tau_0, \mathbf{R}_0)| = \max_\tau\{|s(\tau, \mathbf{R}_0)|\}$.
- the RMS delay spread of $s(\tau, \mathbf{R})$ (on a realization basis),

$$\Delta\tau(\mathbf{R}) = \sqrt{\frac{\int(\tau - \tau_m)^2|s(\tau, \mathbf{R})|^2 d\tau}{\int |s(\tau, \mathbf{R})|^2 d\tau}} \tag{5}$$

  where τ_m is the average delay defined as

$$\tau_m(\mathbf{R}) = \int \tau|s(\tau, \mathbf{R})|^2 d\tau / \int |s(\tau, \mathbf{R})|^2 d\tau.$$

Note that the above definitions assume that the received space-time signal is sampled correctly in time so that the maximal amplitude can be captured. An alternative definition of $\eta(\mathbf{R})$ would be to consider the peak energy, irrespective of the time delay:

$$\eta_M(\mathbf{R}) = \max_\tau\{|s(\tau, \mathbf{R})|^2\}. \tag{6}$$

Both $\eta_D(\mathbf{R})$ or $\eta_M(\mathbf{R})$ and $\Delta\tau(\mathbf{R})$ are random spatial functions, which can be characterized by their first-order moments.

1) Spatial Focusing: The spatial focusing around the focal point is described by two parameters.

The asymptotic space-focusing gain (SFG) is given by

$$p_D = \lim_{|\mathbf{R}-\mathbf{R}_0|\to\infty} \eta_D(\mathbf{R}_0)/\eta_D(\mathbf{R}). \tag{7}$$

It is the ratio between the energy at $\mathbf{R}_0$ to the energy at long distance from $\mathbf{R}_0$. A large value of this ratio indicates better space focusing. Note that p_M is defined similarly with respect to $\eta_M(\mathbf{R})$, and that p_D could be defined at different time delays, i.e. other than τ_0.

The 3-dB contour of the energy function $\eta_D(\mathbf{R})$ or $\eta_M(\mathbf{R})$ can be considered as the focusing region. It is described by the distance in both range and cross-range for which $\eta_D(\mathbf{R})$ or $\eta_M(\mathbf{R})$ remains within 3 dB below the energy at $\mathbf{R}_0$. The characteristic parameters G_a and G_x are therefore defined (e.g. for η_D such that:

$$\eta_D(\mathbf{R}_0 + G_a\mathbf{u}_a)/\eta_D(\mathbf{R}_0) = 0.5 \tag{8a}$$

$$\eta_D(\mathbf{R}_0 + G_x\mathbf{u}_x)/\eta_D(\mathbf{R}_0) = 0.5 \tag{8b}$$

where $\mathbf{u}_a$ and $\mathbf{u}_x$ are unit vectors, respectively in the range and cross-range directions (i.e. in directions respectively parallel and orthogonal to the $\mathbf{T} - \mathbf{R}$ axis).

2) Time Focusing: The time focusing at the focal point is described by the RMS delay spread of $s(\tau, \mathbf{R})$ at $\mathbf{R} = \mathbf{R}_0$, denoted as $\Delta\tau_0 = \Delta\tau(\mathbf{R}_0)$. Note that this delay-spread is expressed in (5), and accounts for the pulse width.

Finally, a time focusing gain (TFG) is also suitably defined by the relative increase of RMS delay spread $\Delta\tau(\mathbf{R})$ at any point $\mathbf{R}$ compared to $\mathbf{R}_0$. The parameter is denoted as

$$\sigma(\mathbf{R}) = \frac{\Delta\tau(\mathbf{R}) - \Delta\tau_0}{\Delta\tau_0} \tag{9}$$

The asymptotic TFG is given by $\lim_{|\mathbf{R}-\mathbf{R}_0|\to\infty} \sigma(\mathbf{R})$. A larger TFG indicates better temporal focusing in the sense that the time compression at the focal point with respect to any point away from the focal point becomes larger.

The performance measures descrived above are random variables, depending on the channel realization. Hence, they should be characterized by their mean and variance taken over all realizations.

B. Measured UWB Channels

In this first part, we present CIRs obtained from TR as computed from real data measured with a very large bandwidth.

1) Experimental Set-Up: Measurements were conducted by Intel Corp. at off-peak hours to ensure channel stationarity. The environment is an office space (40 m × 60 m) with many cubicles. Measurements span the bandwidth 2-8 GHz with 3.75 MHz frequency resolution. Antennas are vertically polarized. The virtual grid on which the receiver is moved has a distance of $\lambda_m/4$ where λ_m is the wave length of the mid frequency of the measurements (5 GHz). The antenna is moved to a different location with a precise robotic positioner. At each antenna position, the channel is measured over a 6 GHz band from 2.0 GHz to 8.0 GHz using a vector network analyser. The measurements are corrected to compensate for the system components (including cable, gain stages, and antennas). The height of the transmit antenna is about 2.5 m and that of the receive antenna is 1m above the floor.

The CIR is computed by taking the inverse DFT of measurement data.

2) Experimental Results: We evaluated η_M for 11 different scenarios. Hereafter, we only consider the two extreme cases which have the worst focusing and yet they are very similar to the outcomes for the other scenarios. The first case is an essentially line-of-sight (LOS) scenario with a transmitter-receiver separation of 3 m. The second case has a separation of 11 m and is a typical non-LOS (NLOS) situation.

A 3D plot of $\eta_M(\mathbf{R})$ of these two cases is shown in Fig. 3. In this figure, the square grid spans a region of $7\lambda_m \times 7\lambda_m$ where $\lambda_m \approx 6$ cm. We see that spatial focusing works fine in both scenarios. In neither of them, however, the peak is isotropic; both peaks have one direction in which they fall off faster, and another, in which the decay is slower. The structure of the peak carries some information about the geometry of the environment, i.e., about directions which show faster and those which show slower decorrelation in space.

The signal power level is at least 10 dB lower at a distance of $7\lambda_m$ than its value at the receiver. This demonstrates the spatial decorrelation very well.

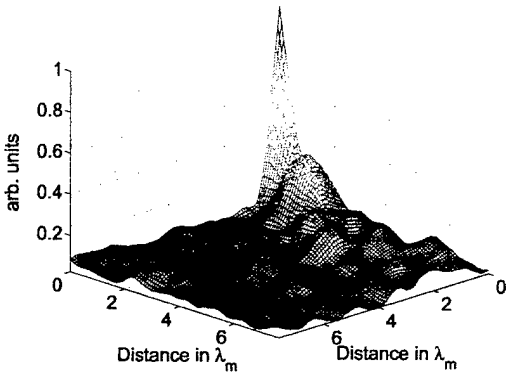

(a) LOS scenario.

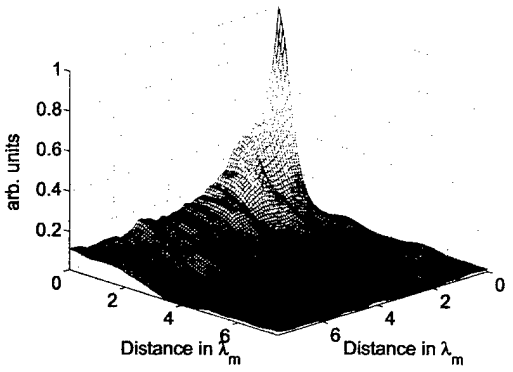

(b) NLOS scenario

Fig. 3. Spatial Focusing $\eta_M(\mathbf{R})$. One shot spatial field realizations for a) the line-of-sight b) the non-line-of-sight scenario.

In Fig. 4 we illustrate the time compression of the received pulse. Displayed are the magitude of the CIR for the LOS scenario (a), the respective time-reversed, i.e., compressed CIR (b), the CIR for the NLOS scenario (c), and the compressed one for this case (d). The channel's power that is not in one (central) tap is significantly shortened. Yet, for the LOS-case, comparably strong side lobes remain visible, since the deterministic component causes correlation. The CIR of the NLOS channel is much better compressed in time. Still, there is some intersymbol interference in the time compressed field and this would require equalizing the received signal. However, the time compressed channel has a significantly less power in its side lobes and is thus less expensive to equalize.

For these two sets of data, we computed the temporal and the spatial focusing gain which are displayed in Tab. I. The TFG is 75% and 30%, respectively, for the LOS and the NLOS case. The CIR with the stronger deterministic component has a higher TFG. The SFG is 21 and 42 so that the SFG in the LOS scenario it is lower. A dominating strong component in the channel yields higher TFG, but lower spatial orthogonality.

To provide a better physical understanding of these observed results, we will present in the following a detailed character-

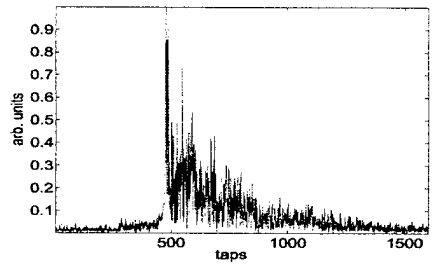

(a) LOS

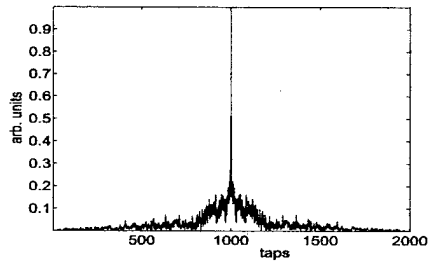

(b) LOS

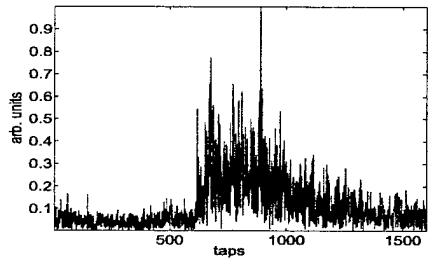

(c) NLOS

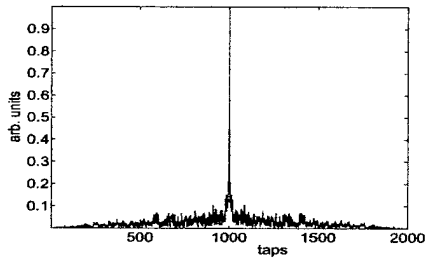

(d) NLOS

Fig. 4. Magnitude of channel impulse responses (a and c) and the time compressed impulse response (b and d)

ization of TR focusing in two different wireless channels at 2.5 GHz: a randomly-filled waveguide and a discrete scattering channel.

C. Random Waveguide

1) Channel Model: We investigate in this section guided wave propagation in two dimensions. The interior of a periodic waveguide is a weakly scattering medium. Signals propagating through this waveguide experience significant multipathing yielding a large delay-spread. This model can seen as an approximation of propagation through hallways inside buildings

TABLE I

TFG AND SFG COMPUTED FROM EXPERIMENTAL DATA.

	TFG (eq. (9))	p_M (eq. (6), (7))
LOS	0.75	21
NLOS	0.31	42

or urban canyons.

Here multipaths are caused by two different mechanisms: reflections from the waveguide walls and scattering by the medium inhomogeneities. Fig. 5 shows a sketch of the waveguide: two rays are propagating from the source at $\mathbf{R}_0$ to the transponder $\mathbf{T}$. One ray reaches $\mathbf{T}$ after several reflections from the waveguide walls. The other one reaches $\mathbf{T}$ by multiple scattering on the inhomogeneities. In fact the source at $\mathbf{R}_0$ produces an entire angular spectrum of rays over the bandwidth, and signals reaching $\mathbf{T}$ undergo a mixture of these two multipathing effects.

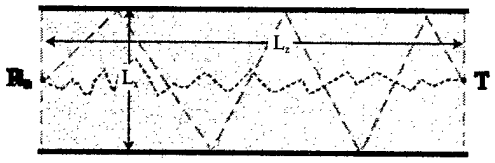

Fig. 5. A sketch of the random waveguide model with two rays from the source at $\mathbf{R}_0$ propagating to the transponder at $\mathbf{T}$ each undergoing one of the two mechanisms for multipathing: reflection from walls and scattering by inhomogeneities.

The waveguide width is L_x and the distance along the waveguide between $\mathbf{R}_0$ and $\mathbf{T}$ is L_z. We assume that the initial transmitted signal at $\mathbf{R}_0$ can be given a limited angular aperture ϑ. For the sake of simplicity, the mean refractive index is chosen as unity (note that changing this value only affects the overall phase of the computation). The fluctuation is an isotropic, Gaussian correlated random function of space, with RMS height h_{RMS} and correlation length ℓ.

To compute the random space-time field, we place equispaced phase screens inside the waveguide separated in distance by ℓ. Simulating propagation along the waveguide involves combining a sequence of steps from one screen to the next. Each step involves propagation through an "empty" waveguide followed by a random phase correction.

We now describe a single step of the phase screen method. Let z_{n-1}, z_n and z_{n+1} denote locations of three consecutive phase screens. We assume that the channel transfer function $H_B(\omega, z_{n-1} \to z_n)$ from z_{n-1} to z_n is known. Because the waveguide is periodic, we express it as a Fourier series:

$$H(\omega, z_{n-1} \to z_n) = \sum_{m=-\infty}^{\infty} a_m(\omega, z_n) e^{j2\pi m x/L_x}. \quad (10)$$

The channel transfer function for z_n to z_{n+1} is then given by

$$H(\omega, z_n \rightarrow z_{n+1}) = e^{jk\tilde{\mu}(x)\delta z/2} \times \left[\sum_{m=-\infty}^{\infty} T_m(\omega, \delta z) a_m(\omega, z_n) e^{j2\pi m x/L_x} \right] \quad (11)$$

with $\delta z = z_{n+1} - z_n$ and $k = 2\pi/\lambda$ the wavenumber. The forward propagation operator $T_m(\omega, \delta z)$ is defined as

$$T_m(\omega, \delta z) = \exp\left[jk\sqrt{1 - (2\pi m/(kL_x))^2}\delta z \right]. \quad (12)$$

The random phase correction $\tilde{\mu}(x)$ is a path-integral of the fluctuation $\mu(x, z) = 1 - n^2(x, z)$ between the screens z_n and z_{n+1} with $n(x, z)$ denoting the index of refraction inside the waveguide.

To limit the angular aperture for the initial transmit at $\mathbf{R}_0$, we filter the Fourier modes before updating the field to the next phase screen. Let z_0 denote the phase screen containing $\mathbf{R}_0$ and $\Psi(\omega, z_0, x)$ denote the initial transmit signal which we express as the Fourier series:

$$\Psi(\omega, z_0, x) = \sum_{m=-\infty}^{\infty} \psi_m(\omega) e^{j2\pi m x/L_x}. \quad (13)$$

From (12) we determine that propagating modes are those for which

$$|m| < \frac{kL_x}{2\pi}. \quad (14)$$

All others are evanescent. For a propagating mode, the propagation angle is determined from $\sin\vartheta_m = 2\pi m/(kL_x)$. The largest value of m such that (14) holds gives the largest propagation angle $\vartheta_{\max}$. To set the angular aperture of the initial transmit ϑ, we restrict the summation in (14) to modes m such that $\vartheta_m \leq \vartheta$.

2) Simulation Results: Numerical simulations in the waveguide have been carried out using the following parameters:

- the central frequency is 2.5 GHz
- the length L_z is 100 m
- the refractive index fluctuation has RMS height $h_{\text{RMS}} = 0.05$ and correlation length $\ell = 1.0$ m
- the waveguide width L_x is either 12.8, 25.6 or 51.2 m
- the source angle ϑ is either 25°, 45° or 65°
- the bandwidth B is between 10 and 100 MHz.

The focus point $\mathbf{R}_0$ is centered in the waveguide. We set $\mathbf{R}_0$ to be the origin for the $x - z$ coordinate system. The transponder is located 100 m down-range from $\mathbf{R}_0$. It is an aperture spanning $1\,\text{m} \leq x \leq 2\,\text{m}$. Note that the aperture center is deliberately slightly skewed from $x = 0$ as to break any symmetry. Hence, any observed effect is by no means an artifact caused by symmetry. Note also that our numerical results have shown that the space-time focusing is insensitive to the location of the transponder array as long as there is sufficient multipathing in the channel.

Figs. 6 and 7 show $\eta_D(x, z_0)/\eta_D(x_0, z_0)$ and $\Delta\tau(x, z_0)$ respectively for a waveguide of width 25.6 m. Averages were computed for 500 realizations of the random refractive index. Results are shown for bandwidths of 10, 20, 40, 80 and 100 MHz.

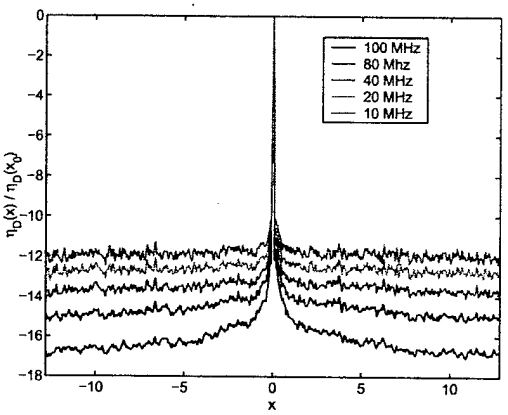

Fig. 6. Energy of $s_B(\tau_0, x)$ in a waveguide with width $L_x = 25.6$ m and $L_z = 100$ m averaged over 500 realizations of the random refractive index. The source is limited in angle by $\Delta\vartheta = 45°$ and in bandwidth by 100, 80, 40, 20 and 10 MHz.

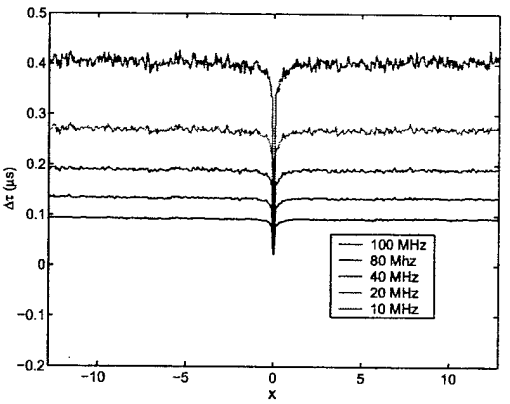

Fig. 7. RMS delay spread τ_{RMS} averaged over 500 realizations of the random refractive index. All other parameters are the same as in Fig. 6.

In Fig. 6 we observe that quality of spatial focus about $x_0 = 0$ is nearly the same over all bandwidths. However, the energy away from the refocus location decreases as the bandwidth increases. In particular, we observe a 5 dB difference between the 10 MHz and 100 MHz cases.

In Fig. 7 we observe the quality of temporal focus about $x_0 = 0$ where $\Delta\tau$ is the smallest. Because a larger bandwidth yields a shorter pulse, $\Delta\tau$ is smaller for larger bandwidths. Nonetheless, the curves become smoother as the bandwidth increases. This phenomenon is due to the onset of statistical stability manifested from broad bandwidth signals [34].

To examine spatial focusing in greater detail, we show the space-focusing gain in Fig. 8. The top plot is for $L_x = 25.6$ m with different values of ϑ. The bottom plot is for $\vartheta = 45°$ with different values of L_x. As we have already mentioned, adding bandwidth to the system reduces the energy away from the refocus location. Fig. 8 further demonstrates this since all curves show that SFG increases with bandwidth. The top plot in Fig. 8 shows that limiting ϑ reduces the SFG. The bottom plot shows that there is little difference between the $L_x = 12.8$

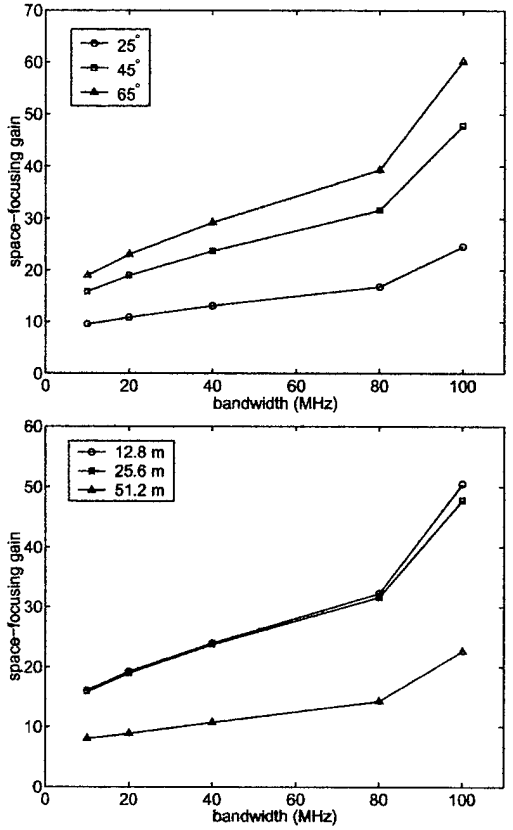

Fig. 8. Asymptotic space-focusing gain (SFG) as a function of bandwidth for different source angles (top) with waveguide width $L_x = 25.6$ m and different waveguide widths (bottom) with source angle $\Delta\vartheta = 45°$.

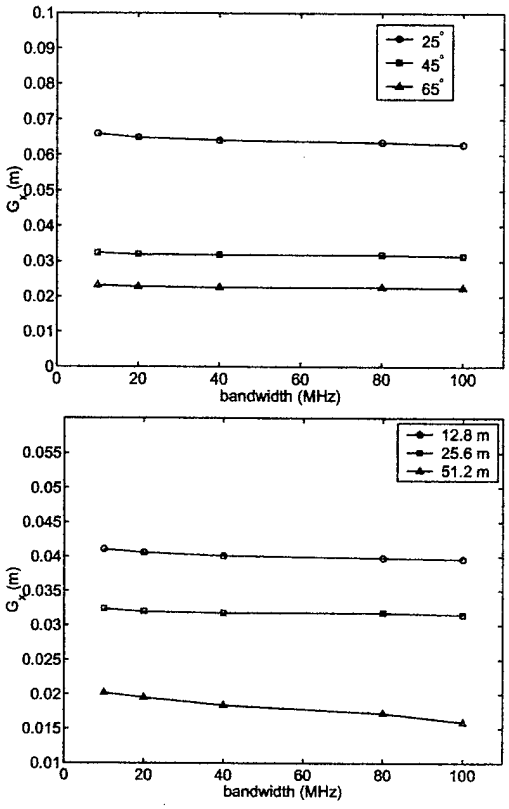

Fig. 9. 3-dB contour in cross-range G_x as a function of bandwidth for different source angles (top) with waveguide width $L_x = 25.6$ m and different waveguide widths (bottom) with source angle $\Delta\vartheta = 45°$.

m and 25.6 m cases. However the SFG for the $L_x = 51.2$ m case is much smaller than the other two. For a fixed ϑ, widening the waveguide reduces the diversity of modes that propagate in the channel. This reduction, in turn, reduces the quality of focus in time reversal.

In addition, we show the 3-dB contour in cross-range G_x in Fig. 9. Similar to Fig. 8, the top plot is for $L_x = 25.6$ m with different values of ϑ and the bottom plot is for $\vartheta = 45°$ with different values of L_x. Here we observe that cross-range dependence of the 3-dB contour changes very little with respect to bandwidth. Because limiting the angular aperture of the source is a spatial low-pass filter yielding broader initial transmit sources, G_x increases as ϑ decreases. For different waveguide widths, the 3-dB contour does not change significantly. It decreases slightly as the width increases because of added angular diversity. From (14) we understand that the number of propagating modes within a fixed angular aperture is set by λ and L_x. With λ fixed and L_x increasing, more propagating modes exists inside the angular aperture. For example, with $\vartheta = 45°$, there are approximately 75, 150 and 301 propagating modes for $L_x = 12.8$ m, 25.6 m, and 51.2 m, respectively. Time reversal methods exploit this added spatial diversity to tighten the refocusing.

To examine temporal focusing more closely, we show the asymptotic limit of the time-focusing gain in Fig. 10. The top plot is for $L_x = 25.6$ m with different values of ϑ and the bottom plot is for $\vartheta = 45°$ with different values of L_x. All curves decrease monotonically with bandwidth. The main reason for this decrease is that the pulse is narrower as bandwidth increases. The overall delay spread is reduced and the refocus region is not as pronounced. The TFG increases with ϑ since the additional diversity allows for greater temporal focusing in the sense that ratio between $\Delta\tau$ at and away from x_0 becomes greater. Similar to the result for the SFG, we observe that the TFG for $L_x = 12.8$ m and 25.6 m are close to each other while the widest waveguide yields a smaller TFG. As L_x increases effects manifested by reflections from waveguide walls decrease and the waveguide domain approaches an unbounded one exhibiting a smaller TFG.

D. Geometry-Based Stochastic Channel

1) Channel Model: For discrete scattering media, such as typical outdoor wireless environments, the channel can be represented by a number of effective scatterers randomly distributed in space. A ray-based approach can then be used to describe the channel as a sum of so-called scattered or reflected

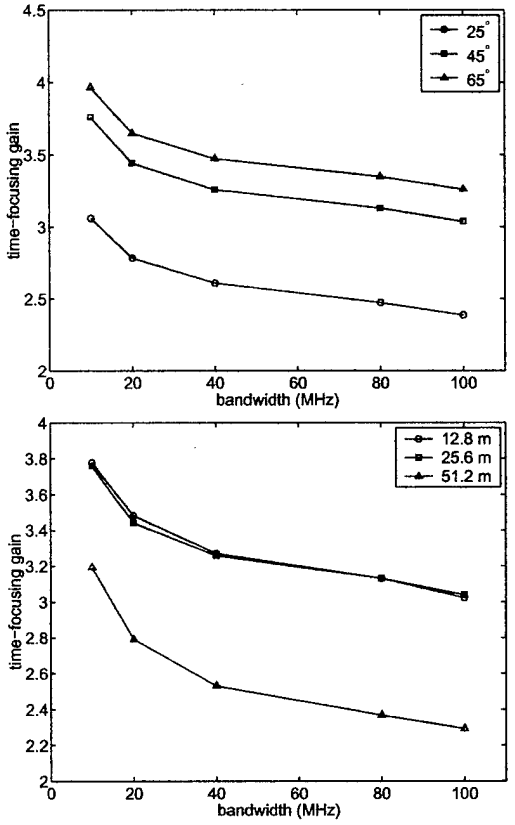

Fig. 10. Asymptotic time-focusing gain (TFG) as a function of bandwidth for different source angles (top) with waveguide width $L_x = 25.6$ m and different waveguide widths (bottom) with source angle $\Delta\vartheta = 45°$.

contributions. In the following, the statitical distribution of scatterers is based on the well-known one-ring model [30].

We first consider that only single scattering occurs. We assume that the scatterers are uniformly distributed inside an annular region surrounding the target point, as illustrated in Fig. 11. This region is specified by a minimal radius ρ_m and a maximal radius ρ_M. The angle-spread of the channel (as seen from the target point) is fixed by limiting the aperture of the annular region to a given portion, i.e. specifying minimum and maximum angles, ϑ_m and ϑ_M (see Fig. 11). In this paper, we refer to $\Delta\vartheta = \vartheta_M - \vartheta_m$ as the scattering angle-spread or simply the angle-spread.

We further simplify the channel description by choosing $\rho_M = 2\rho_m$ and $\rho_M << D$, with D denoting the distance between the transmit and target points. Hence, the RMS delay spread of the physical channel (over an infinite bandwidth) is well approximated for an omnidirectional distribution of scatterers ($\Delta\vartheta = 2\pi$) by

$$\tau_{\text{RMS}} \approx \frac{\sqrt{5}\rho_m}{2c} \tag{15}$$

with $c = 3 \times 10^8 m/s$ is the speed of light. For a limited angle spread, we assume that $\vartheta_m = \pi - \Delta\vartheta/2$ and $\vartheta_M = \pi + \Delta\vartheta/2$.

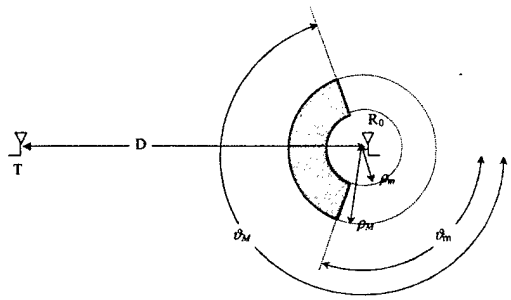

Fig. 11. Geometrical representation of the propagation model.

In that case, the delay-spread can be written as

$$\tau_{\text{RMS}} \approx \frac{\sqrt{5}\rho_m}{2c}\sqrt{\frac{\Delta\vartheta + \sin\Delta\vartheta}{2\pi}} \tag{16}$$

The channel transfer function is easily estimated by means of a ray-tracing approach that yields

$$\begin{aligned} H(\omega, \mathbf{R}_0) &= \sum_{l=1}^{N} G(\omega, \mathbf{R}_0 \to \mathbf{S}_l)\Gamma_l \\ &\quad \times \left[\frac{d_{\mathbf{R}_0\mathbf{S}_l} d_{\mathbf{S}_l\mathbf{T}}}{d_{\mathbf{R}_0\mathbf{S}_l} + d_{\mathbf{S}_l\mathbf{T}}}\right]^{\gamma/2} G(\omega, \mathbf{S}_l \to \mathbf{T}) \quad (17) \\ &= \sum_{l=1}^{N} \Gamma_l \frac{\exp\left[-j\omega(d_{\mathbf{R}_0\mathbf{S}_l} + d_{\mathbf{S}_l\mathbf{T}})\right]}{[d_{\mathbf{R}_0\mathbf{S}_l} + d_{\mathbf{S}_l\mathbf{T}}]^{\gamma/2}}. \quad (18) \end{aligned}$$

The quantities in (17) and (18) are

- $\omega = 2\pi/\lambda$, the angular frequency (λ denoting the wavelength);
- $G(\omega, \mathbf{P} \to \mathbf{Q}) = \exp(-j\omega d_{\mathbf{PQ}})/(d_{\mathbf{PQ}})^{\gamma/2}$, the spreading function for a transmission from $\mathbf{P}$ to $\mathbf{Q}$, with γ denoting the path-loss exponent ($\gamma = 2$) and $d_{\mathbf{PQ}}$ denoting the distance between $\mathbf{P}$ and $\mathbf{Q}$;
- Γ_l, the scattering coefficient of the l^{th} scatterer; in this paper, it is considered to be a complex Gaussian variable, with given standard deviation;
- $\left[\frac{d_{\mathbf{R}_0\mathbf{S}_l} d_{\mathbf{S}_l\mathbf{T}}}{d_{\mathbf{R}_0\mathbf{S}_l} + d_{\mathbf{S}_l\mathbf{T}}}\right]^{\gamma/2}$ is the usual spreading factor for reflection [32], ensuring that the transfer function is inversely proportional to the total distance, as outlined by (18); multiplying this reflection spreading factor by Γ_l yields the so-called scattering cross-section.

Note that (17) and (18) implicitly assume that the CIR is filtered by a Nyquist filter with roll-off factor equal to zero, hence the filter is a rectangular window in the frequency domain. Simulations were done with the following parameters:

- the central frequency is 2.5 GHz;
- the transponder is separated from the target point by a distance of 10^4 wavelengths, i.e. 1.2 km;
- when the delay-spread is not used as a variable or explicitely assigned a specific value, it is fixed at 0.8μs (i.e. $\rho_m = 1800\lambda$);
- different angle spreads, ranging from $\pi/3$ to 2π.
- the scattering coefficient is assumed to be complex Gaussian distributed with standard deviation of 0.25.

2) Omnidirectional Scattering Results: Fig. 12 shows snapshots of $\eta_D(\mathbf{R})$ (the target point is in the center of the figure), for two bandwidths: 50 and 100 MHz, two channel delay spreads and omnidirectional angular spreading of the scatterers.

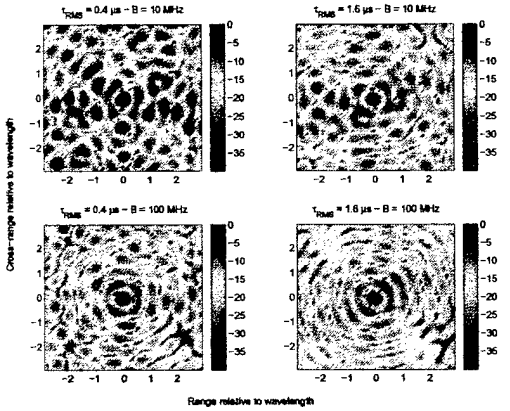

Fig. 12. Typical one-shot realizations of time reversed random fields (the energy function is expressed in [dB]).

The impact of both the bandwidth and the channel delay-spread is clearly visible (the scales are kept constant from graph to graph). For the smallest $B \times \tau_{\text{RMS}}$ product, some areas receive the same level of energy as the target point. For the largest $B \times \tau_{\text{RMS}}$ product, the space focusing gain is about 15 to 20 dB. Also, it seems that the instantaneous energy function is oscillating as a function of the distance to the focal point.

Fig. 12 shows that the space-time focusing is improved when both the bandwidth and the delay-spread are increased. Figs. 13 and 14 show $E\{\eta_D(\mathbf{R})/\eta_D(\mathbf{R_0})\}$ and $E\{\Delta\tau(\mathbf{R})\}$ as a function of the system bandwidth. The channel delay spread is set to 0.8 μs for these simulations.

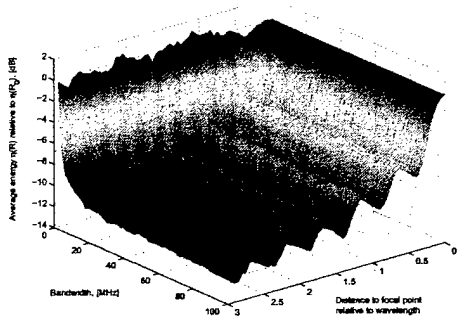

Fig. 13. Simulated energy function $E\{\eta_D(\mathbf{R})/\eta_D(\mathbf{R_0})\}$ as a function of range and bandwidth ($\tau_{\text{RMS}} = 0.8\mu$s).

The simulated dependencies have been fitted by the following empirical formulas:

$$E\{p_D\} = \bar{p}_D = 5.9\tau_{\text{RMS}}^{0.29} B^{0.35} \tag{19}$$

$$E\{p_M\} = \bar{p}_M = 2.2\tau_{\text{RMS}}^{0.24} B^{0.52} \tag{20}$$

$$E\{\frac{\eta_D(\mathbf{R})}{\eta_D(\mathbf{R_0})}\} \cong K_D + (1 - K_D) \times |J_0(2\pi|\mathbf{R} - \mathbf{R_0}|/\lambda)|^{\alpha} \exp(-|\mathbf{R} - \mathbf{R_0}|/3.2\lambda) \tag{21}$$

with

$$\alpha = 2.6\exp(-\tau_{\text{RMS}}/1.23) \tag{22}$$

and

$$K_D \propto 1/\bar{p}_D \tag{23}$$

$$\bar{G}_a/\lambda = \bar{G}_x/\lambda = 0.41\tau_{\text{RMS}}^{-0.01} B^{-0.02} \tag{24}$$

$$\overline{\Delta\tau_0} = 0.083\tau_{\text{RMS}}^{-1.25} B^{-1} + 0.93\tau_{\text{RMS}}^{0.92} \tag{25}$$

$$E\{\sigma(\mathbf{R})\} \cong 0.37\{1 - |J_0(2\pi|\mathbf{R} - \mathbf{R_0}|/\lambda)|^{\beta} \times \exp(-|\mathbf{R} - \mathbf{R_0}|/1.5\lambda)\} \tag{26}$$

with $\beta = 1.3\exp(-\tau_{\text{RMS}}/1.8)$. Here, the bandwidth B is expressed in MHz, and the delay-spread τ_{RMS} is expressed in μs.

The alternative energy ratio $E\{\eta_M(\mathbf{R})/\eta_M(\mathbf{R_0})\}$ can be expressed in the same fashion as in (21).

- In (19), (24) and (25), exponents for B and τ_{RMS} are similar when both variables appear multiplied by each other. This observation implies that space-time focusing in general is improved by increasing the product $B \times \tau_{\text{RMS}}$. However, that assertion should be nuanced, since some terms in (25) and (26), as well as α and β are only related to the channel delay-spread.
- When B is sufficiently large (> 10), the space-focusing parameters depend upon $B \times \tau_{\text{RMS}}$. This impact is significant regarding the asymptotic SFG. However, the dependence of the 3-dB contour width towards $B \times \tau_{\text{RMS}}$ is much weaker. Both G_a and G_x are therefore mostly inversely proportional to the carrier frequency only. Note that for smaller bandwidths (for which eqs. (19) and (20) are not valid anymore), the average asymptotic SFG tends to unity.
- The average delay spread at the focal point $\overline{\Delta\tau_0}$ results from the additive combination of two terms: one roughly related to $B \times \tau_{\text{RMS}}$, and the other one to τ_{RMS} only. For large $B \times \tau_{\text{RMS}}$, the variation of $\overline{\Delta\tau_0}$ with B becomes weak, so $\overline{\Delta\tau_0}$ only depends upon the channel delay-spread. This is clearly visible on Fig. 14. At any other point $\mathbf{R}$ outside the focusing region, the average delay spread $E\{\Delta\tau(\mathbf{R})\}$ is an oscillating increasing exponential function of the distance from the focal point. It saturates at long distances.
- At any point $\mathbf{R}$, the time-focusing gain $E\{\sigma(\mathbf{R})\}$ is only related to the channel delay-spread. Furthermore, the asymptotic TFG (i.e. at long distance) is a constant value (~ 0.37) independent from B and τ_{RMS}, at least for sufficiently large $B \times \tau_{\text{RMS}}$ (> 10).

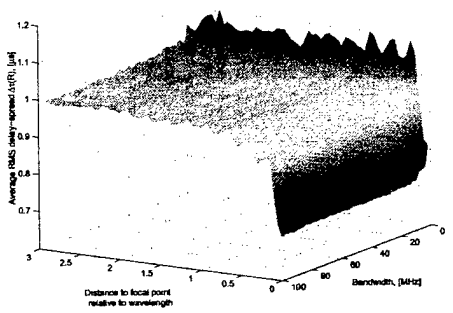

Fig. 14. Simulated RMS delay spread $E\{\Delta\tau(\mathbf{R})\}$ as a function of range and bandwidth ($\tau_{\text{RMS}} = 0.8\mu$s).

3) Impact of Reduced Angular Spread: When the angle spread is decreased from 2π to smaller angles, the spatial focusing is degraded as expected.

- For $\Delta\vartheta > \pi/3$, the asymptotic SFG $\bar{p}_D$ decreases as $\Delta\vartheta$ decreases, and is found to vary as $(\Delta\vartheta/2\pi)^{0.6}$.
- The 3-dB contours $\bar{G}_a$ and $\bar{G}_x$ are not identical anymore, and $\bar{G}_a \cong 4\bar{G}_x$ for $\Delta\vartheta \leq 3\pi/4$. They are decreased respectively by $\Delta\vartheta^{-1.3}$ and $\Delta\vartheta^{-1.2}$ relatively from their previous values (i.e. when $\Delta\vartheta$ was equal to 2π). For $\Delta\vartheta > 3\pi/4$, the ratio $\bar{G}_a(\Delta\vartheta)/\bar{G}_a(\Delta\vartheta = 2\pi)$ continues to decrease following a $\Delta\vartheta^{-1.3}$ law while $\bar{G}_x(\Delta\vartheta)/\bar{G}_x(\Delta\vartheta = 2\pi)$ remains constant. Hence, $\bar{G}_a = \bar{G}_x$ for $\Delta\vartheta = 2\pi$.

New empirical expressions can therefore be derived easily that take into account that the channel delay spread τ_{RMS} is also modified when reducing the angle spread, as highlighted by (15) and (16):

$$\bar{p}_D = 5.9\tau_{\text{RMS}}^{0.29} B^{0.35} (\Delta\vartheta/2\pi)^{0.6} \nu^{-0.2} \tag{27}$$

with $\nu = (\Delta\vartheta + \sin\Delta\vartheta)/(2\pi)$,

$$\begin{aligned} \bar{G}_a/\lambda &= 0.41\tau_{\text{RMS}}^{-0.01} B^{-0.02} (\Delta\vartheta/2\pi)^{-1.3} \nu^{0.005} \\ &\approx 0.41(\Delta\vartheta/2\pi)^{-1.3} \end{aligned} \tag{28}$$

$$\begin{aligned} \bar{G}_x/\lambda &= \begin{cases} 0.13\tau_{\text{RMS}}^{-0.01} B^{-0.02} (\Delta\vartheta/2\pi)^{-1.2} \nu^{0.005}, \\ \qquad\qquad \pi/3 \leq \Delta\vartheta \leq 3\pi/4, \\ 0.41\tau_{\text{RMS}}^{-0.01} B^{-0.02} \nu^{0.005}, \quad \Delta\vartheta > 3\pi/4 \end{cases} \\ &\approx \begin{cases} 0.13(\Delta\vartheta/2\pi)^{-1.2}, & \pi/3 \leq \Delta\vartheta \leq 3\pi/4, \\ 0.41(\Delta\vartheta/2\pi)^{-1.3}, & \Delta\vartheta > 3\pi/4. \end{cases} \end{aligned} \tag{29}$$

4) Benefits from Multiple Antennas: The impact of using multiple antennas at the transmit point is analyzed in the following. At the transmit point, the terminal now consists of M_T antennas. Each antenna has a specific location around $\mathbf{T}$, denoted as $\mathbf{T}_u$. Hence, the focused signal is written as

$$s(\tau, \mathbf{R}_0) = \frac{1}{\sqrt{M_T}} \sum_{u=1}^{M_T} h(\tau, \mathbf{R}_0 \to \mathbf{T}_u) \star h(-\tau, \mathbf{R}_0 \to \mathbf{T}_u) \tag{30}$$

where the scaling factor $1/\sqrt{M_T}$ ensures that the total transmitted power is kept constant, irrespective of the number of antennas.

The benefit from multiple antennas is proportional to M_T as far as the SFG is concerned, in agreement to well-known diversity results [31]. Indeed, considering a constant transmitted power, the peak energy at the focal point will grow as M_T, but will remain the same anywhere else outside the focusing region.

5) Multiple-Bounce Model: Single-bounce models are not sensitive to the order of magnitude of Γ and γ since they are only responsible for a proportionality factor. This is not the case for multiple-bounce models in which the average loss per interaction, related to the scattering cross-section and the path-loss, is a critical parameter.

The model can be easily extended to consider multiple bounce interactions. In such case, the transmitted waves are scattered from one to a certain number of times. The calculation of the transmission channel can be written as a sum of N scattered contributions:

$$H(\omega, \mathbf{R}_0) = \sum_{l=1}^{N} C_l \eta_l G(\omega, \mathbf{S}_l \to \mathbf{T}) \tag{31}$$

where

- $G(\omega, \mathbf{S}_l \to \mathbf{T})$ is the spreading function for a transmission from the l^{th} scatterer to the target point $\mathbf{T}$,
- η_l is the scattering cross-section of the l^{th} scatterer, proportional to the scattering coefficient Γ_l [33],
- C_l is the l^{th} element of vector $\mathbf{C}$, which is the solution of a N-order linear system given by:

$$\mathbf{C} = \mathbf{A}^{-1} \cdot \mathbf{C}_0 \tag{32}$$

with

- $C_{0l} = G(\omega, \mathbf{R}_0 \to \mathbf{S}_l)$ is the channel between the target point and the location of each scatterer,
- $\mathbf{A}$ is the system matrix accounting for the transmission between each pair of scatterers:

$$A_{kl} = \begin{cases} \Gamma_k G(\omega, \mathbf{S}_k \to \mathbf{S}_l) & k \neq l, \\ 1 & k = l. \end{cases} \tag{33}$$

As already mentioned, this model is highly sensitive to the average loss per interaction, i.e. to the product $|\eta_k G(\omega, \mathbf{S}_k \to \mathbf{S}_l)|$. On one hand, if the latter is very small, then the delay-spread of the channel tends to be infinite, which is unrealistic. On the other hand, if the loss per interaction is very large, the impact of high-order scattered contributions becomes small, and the received field is very similar to the first-order field. A reasonable assumption is that contributions up to the third order can be significant. The average loss per interaction should then be chosen accordingly. For an average loss per additional reflection of 12 dB, the impact of multiple reflections on the focusing is negligible. If the average loss per interaction is decreased by 4 dB, the impact, though not negligible, remains small. This is mostly because the large number of scatterers enables the time-reversed field to be highly focused with single-bounce interactions.

6) Comparison with Random Waveguide Model: In both models, the space-focusing gain increases with bandwidth. In the geometry-based model, it is also shown that the SFG increases similarly with the channel delay-spread. In the waveguide model, simulation results illustrate that the SFG also increases with the channel delay-spread. The increase for the waveguide is related to the source angle and to the inverse of the waveguide width. Time-focusing gain examined using the 3-dB contour shows a weak dependence on bandwidth in both scenarios. Similarly, the dependence on the channel delay-spread is also weak, but the 3-dB contour decreases as the angle-spread increases. This is clear in the geometry-based model. In the waveguide model, we have observed that the dependence toward the waveguide width is weak, while there is a noticeable dependence on the angle-spread.

Some differences between these two models have been observed. The most pronounced one is that the SFG appears to be independent of the bandwidth in the case of the discrete scattering model, while a significant dependence is found in the waveguide. Also, the absolute value of the SFG is much larger in the waveguide scenario. To better understand this difference, we need to refer to the specifics of the models. In the waveguide case, two mechanisms cause delay-spread: large-scale multipath results from the coherent reflections by the waveguide walls, small-scale multipath is caused by the non-homogeneities of the refractive index. By contrast, the geometry-based propagation only consists of non-coherent reflections, similar to the waveguide small-scale multipathing. Focusing in time reversal is enhanced for bounded domains in that it is more robust. This accounts for the difference seen in these two models. As the waveguide width approaches infinity, it begins to agree with an unbounded medium.

7) Space-time focusing in time-reversed transmissions: So far, we have assumed that a single time-reversed pulse is sent from the transmitter to the target point. However, in Section V, we will deal with data transmissions in TR schemes. As a preliminary study, we analyze here how space-time focusing is affected when sending a time-reversed data signal. The latter consists of the convolution of the time-reversed pulse with a train of information bits.

Fig. 15 shows the SFG as a function of the relative data rate (i.e. the data rate relative to the pulse bandwidth) for two different Nyquist roll-off factors. The bandwidth is equal to 40 MHz and the channel RMS delay-spread to 0.8μs. For these values the single-pulse SFG $\bar{p}_D \approx 13$ dB. It is clear from Fig. 15 that for the full rate the space focusing advantage is totally destroyed. The same conclusion applies regarding the TFG, as depicted in Fig. 16. In other words, for a single user, the time compression effect resulting from TR is significantly reduced if the rate is not seriously decreased.

In fact, Fig. 15 and 16 show that space and time focusing are slowly restored as the data rate decreases. As an example, the SFG is about 5 to 6 dB for a rate of $B/10$, while the TFG is around 0.22 for that same rate. For higher roll-off factor, the degradation is less than for the zero roll-off case. This is not surprising since higher roll-off factors yield lower side lobes.

Therefore, there is a fundamental trade-off between the data rate and the space-time focusing effect that can be achieved in a wireless channel for a given bandwidth. This trade-off is dictated by the coherence bandwidth of the channel transfer function and is analyzed in more detail in the next section.

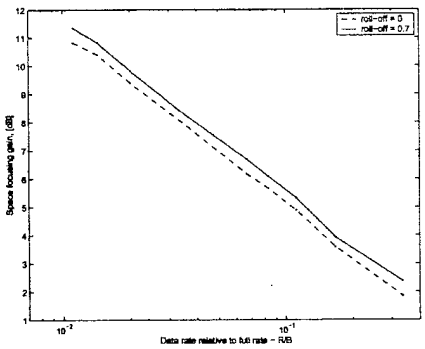

Fig. 15. Spatial focusing gain as a function of data rate and roll-off factor.

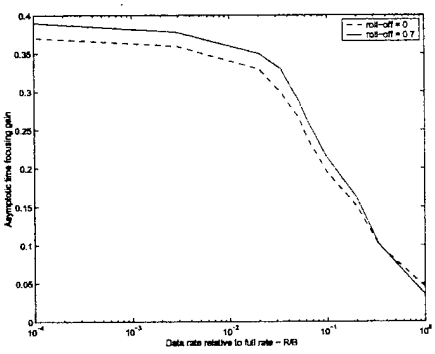

Fig. 16. Time focusing gain as a function of data rate and roll-off factor.

V. Communications over Large Delay Spread Channels with Very Simple Receivers

In this section, we investigate the performance of a most simple TR communication system. We assume that the channel shortening achieved by TR is all that is done to combat remaining ISI in the channel and investigate an uncoded MISO system that employs a simple one-tap receiver without any further equalization. We study the performance of this TR system in the limit of very low and of infinite delay spread. We compare this performance to that of an optimized preequalizer, and examine the impact of the number M_T of transmit antennas, and of a strategy called rate back-off that can combat remaining ISI in the channel in a very simple way. The goal of this study is two-fold. We obtain a lower bound on the performance of a TR communication system in channels with very high delay spread, since any other system that does employ coding or equalization at the receiver will perform better. Note that the upper performance bound was presented in Section III, since the computation of the system's rate in that section assumed both infinitely complex transmitter and receiver and perfect coding. Secondly, the proposed setup can

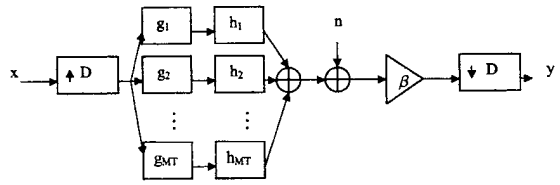

Fig. 17. A block diagram of a MISO system with a preequalizer at the transmitter and a single tap receiver.

be of interest by itself for systems that operate with very large banwidths, not too high data rates, and that rely on extremely simple receiver architectures.

Fig. 17 depicts a block diagram of the system. A symbol x is upsampled by a factor of D, put on the M_T branches to the transmit antennas, filtered with a function g_i which can possibly be a TR prefilter, and sent over the channels h_i. After receive noise is added, the signal can be enhanced by a gain β, and it is downsampled before detection.

For all plots shown in this section, we use a Rayleigh fading channel with L=100 i.i.d. taps.

A. Optimal Prefiltering

First we derive the optimal prefilter for the system in Fig. 17. We describe the input-output relation of the system in matrix form as

$$y[k] = \beta \mathbf{x}_k \mathbf{H}\mathbf{g} + \beta n[k] \tag{34}$$

where $\mathbf{x}_k = [x_1 x_2 \dots x_{2L-1}]$ is a vector of input symbols, $y[k]$ the output symbol and $n[k]$ the noise. The discrete time channel matrix $\mathbf{H}$ is block toeplitz; its block-columns are comprised of the shifted channel vectors $[h_i[1], \dots, h_i[L]]$, and in each block columns that belong to adjacent antennas are next to each other. The vector $\mathbf{g}$ is given by

$$\mathbf{g} = [\mathbf{g}[0]^T \quad \dots \quad \mathbf{g}[L-1]^T]^T \tag{35}$$

and

$$\mathbf{g}[l] = [g_1[l] \quad \dots \quad g_{M_T}[l]]^T \quad l = 0, \dots, L-1. \tag{36}$$

The product $\mathbf{Hg}$ is the convolution of the prefilter and the channel; ^{T} denotes the transpose.

We give here the optimal $\mathbf{g}$ and β for the case of $D = 1$ (no upsampling). In order to simplify receiver processing, the purpose of the set of transmit filters $\mathbf{g}$ is to preequalize the signal. This means that at the receiver, as much power as possible is focused in the central peak, and that ISI is minimized, subject to the power constraint $\| \mathbf{g} \| = 1$ where $\| \cdot \|$ denotes the norm. Such a problem can be stated as an optimization problem, whose solution is

$$\hat{\mathbf{g}} = \frac{1}{\beta} \left(\mathbf{H}^H \mathbf{H} + \frac{\sigma^2}{P_{T_x}} \mathbf{I} \right)^{-1} \mathbf{H}^H \hat{\mathbf{e}}_\Delta \tag{37}$$

$$\beta^2 = \hat{\mathbf{e}}_\Delta^T \mathbf{H} \left(\mathbf{H}^H \mathbf{H} + \frac{\sigma^2}{P_{T_x}} \mathbf{I} \right)^{-2} \mathbf{H}^H \hat{\mathbf{e}}_\Delta. \tag{38}$$

Δ is the delay of the equalizer, and $\hat{\mathbf{e}}_\Delta$ the unit vector with 1 in entry Δ, and $P_{T_x} = E[\mathbf{x}_k^T \mathbf{x}_k]$. Eq. (37) defines a filter

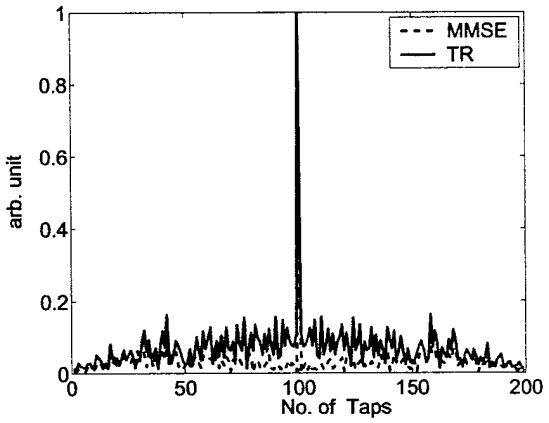

Fig. 18. The focused CIR for the TR- and the optimal prefi lter.

with an MMSE-type solution with a finite number of taps. We notice that the optimized value for β bascially ensures that the power constraint of the filter is valid. In the transmit-receiver chain of Fig. 17, β has no effect on the SNR at the receiver; it ensures, however, that the transmitter can take into account the SNR to optimize the preequalizer. We note that even though there exists a striking similarity to an MMSE receiver, we could not establish the convexity of the optimization problem. Hence, our solution (37) may actually only be a local optimum. The similarity of the solution to the MMSE receive equalizer suggests that the found optimum shows good performance; but better solutions may exist.

The TR-prefilter is a matched prefilter; it follows from the optimal filter (37) for low SNR,

$$\mathbf{g}_{TR} = \lim_{SNR \to 0} \mathbf{g} = \mathbf{h}^* \quad s.t. \ \| \mathbf{h} \| = 1, \tag{39}$$

or

$$g_{TR,i}[k] = \sqrt{\gamma} h_i^*[-k],$$

with $\gamma = \left(\sum_{i=1}^{M_T} \sum_{l=0}^{L-1} |h_i[l]|^2 \right)^{-1}$, i.e., the filter equals the time-reversed CIR of the channel, and the receiver receives the autocorrelation function of the channel. The power in its central peak is maximized, but the ISI suppression is worse.

A picture of the CIRs that result from precoding with the optimal and the TR strategy is shown in Fig. 18. The SNR is 10 dB. The optimal prefilter suppresses the ISI better than the TR prefilter; close inspection reveals that the power in the peak of the CIR is slightly higher in case of TR. The improved ISI suppression in case of the optimal prefilter comes at computational cost. The optimal transmit prefilter requires a matrix inversion which can be difficult if the number of channel taps is too high or the channel is not sufficiently stationary.

B. Rate Back-off

Fig. 18 suggests that the application of TR or even of an optimized prefilter with a single antenna leaves considerable

residual ISI in the channel. One method to combat ISI is to transmit at lower rate; if the transmission rate is by a factor of D lower than the bandwidth of the channel, the ISI is on average also reduced by a factor of D, but the useful power, concentrated in the peak of the CIR, remains constant. Such a strategy is not favorable if high spectral efficiency is required. But for systems which operate at very large bandwidths, such as ultra-wideband systems, it can be very attractive to trade abundantly available transmission bandwidth against complexity.

Rate back-off by a factor of D is equivalent to upsampling the signal before transmission, and downsampling it by D before detection. The input-output relation of the pre-equalized channel with rate back-off factor D, $D = 1, \ldots, L$, can be derived as

$$y^{[D]}[k] = \beta \sum_{i=1}^{M_T} \sum_{l} (h_i \star g_i)[Dl] x[k-l] + \beta n[k] \qquad (40)$$

where $x[k]$ is the input symbol and $y^{[D]}[k]$ the output symbol received with rate back-off. We see that the rate back-off yields an equivalent channel which is sampled only at each Dth instant.

C. Focusing Ratio and Effective SNR

1) Definitions: We introduce some performance measures that we will later use for system characterization. A very intuitive performance measure is the focusing ratio κ which we define as

$$\kappa = \frac{E[P_0]}{E[Q^{[D]}]} \qquad (41)$$

where $E[P_0]$ is the expected power in the central peak of the preequalized CIR, and $E[Q^{[D]}]$ is that of the ISI with rate back-off D, i.e., the power in the tails of the preequalized CIR. The better the focusing, the larger is κ. Unlike the measure introduced in (9), the measure here takes into account the entire, temporally spread power of the received signal, and not just the ratio of the energies of the maximum and of one distant tap.

We can express the power of the received, possibly downsampled, signal as

$$E[|y^{[D]}[k]|^2] = P_{Tx} E[P_0] + P_{Tx} E[Q^{[D]}] + \sigma^2 \qquad (42)$$

where we used $E[x[l]x[m]] = P_{Tx}\delta[l-m]$, with P_{Tx} denoting the transmitter power, and $E[n[l]n^*[m]] = \sigma^2\delta[l-m]$ with σ^2 the noise power and $\delta[l-m]$ the Kronecker Delta. The constants P_0 and $Q^{[D]}$ are given as [29]

$$P = \left| \sum_{i=1}^{M_T} \sum_{l=0}^{L-1} h_i[l] g_i[-l] \right|^2 \qquad (43)$$

$$Q^{[D]} = \left| \sum_{i=1}^{M_T} \sum_{l \neq 0} \sum_{k \neq 0} h_i[l] g_i[m] \delta[Dk - m - l] \right|^2 . \qquad (44)$$

We define the effective SNR ρ_{eff} as

$$\rho_{eff,D} = \frac{P_{Tx} E[P_0]}{P_{Tx} E[Q^{[D]}] + \sigma^2} = \frac{E[P_0]}{E[Q^{[D]}] + \frac{1}{\rho}} \qquad (45)$$

where $\rho = \frac{P_{Tx}}{\sigma^2}$.

We furthermore define the SNR ρ_{MFB} that would be obtained if there was no precoding but the receiver had a matched filter and used full channel knowledge as

$$\rho_{MFB} = \frac{P_{Tx} E[\sum_{i=1}^{M_T} \sum_{l} |h_i[l]|^2]}{\sigma^2}. \qquad (46)$$

2) Application to TR Systems: The simplicity of the TR prefilter allows to compute the ratio κ of the useful power against the ISI for an exponentially decaying channel with delay spread σ_τ. One obtains in the limit of large L/σ_τ [29]

$$\kappa_{TR} = \left(1 - \exp -\frac{D}{\sigma_\tau}\right) \times \frac{\left[M_T^2 (1 + \exp -\frac{1}{\sigma_\tau}) + M_T (1 - \exp -\frac{1}{\sigma_\tau})\right]}{2 M_T \exp -\frac{D}{\sigma_\tau} \left(1 - \exp -\frac{1}{\sigma_\tau}\right)}. \qquad (47)$$

Using (47) together with (45) and (46) we arrive at an analytical expression for the effective SNR of a TR communication system with M_T transmit antennas and a rate back-off of D,

$$\rho_{eff,D} = \rho_{MFB} \frac{1}{1 + \frac{\rho_{MFB}}{\kappa_{TR}}}. \qquad (48)$$

We can derive from this the following limiting cases:

$$\rho_{eff,D} = \rho_{MFB} \quad \text{for } \sigma_\tau \longrightarrow 0 \qquad (49)$$

$$\rho_{eff,D} = \frac{\rho_{MFB} D M_T}{\rho_{MFB} + D M_T} \quad \text{for } \sigma_\tau \longrightarrow \infty \qquad (50)$$

Eq. (50) can be split into a low-SNR and a high-SNR regime as

$$\rho_{eff,D} = \rho_{MFB} \quad \text{for } \rho_{MFB} \text{ low}, \sigma_\tau \text{ large} \qquad (51)$$

$$\rho_{eff,D} = D M_T \quad \text{for } \rho_{MFB}, \sigma_\tau \text{ large}. \qquad (52)$$

Interpretation of these equations yields the following conclusions:

- Eq. (49) tells that a TR system is lossless if the delay spread of the channel is very small. Preequalization of the channel does hardly change the performance if the delay spread is very small. We recall from Fig. 2, however, that the system in this case is subject to fading which will reduce the rate.
- Eq. (51) shows that TR is optimal at low SNR; this behavior is expected for a transmit matched filter which maximizes the power in the peak of the signal.
- Eq. (52) demonstrates that in an environment with a large delay spread, the performance of a TR system at high input SNR saturates at a value independent from the delay spread of the channel. The performance increases with 3 dB per added transmit antenna, and with another 3 dB for each rate back-off by a factor 2 from the maximum available bandwidth.

The last property is remarkable, because it holds for an uncoded system with no receive equalizer, a fairly simple transmit equalization strategy, and arbitrary delay spread, i.e., arbitrary bandwidth. In a 1 GHz time-invariant channel, a system with a powerful two-antenna transmitter can theoretically

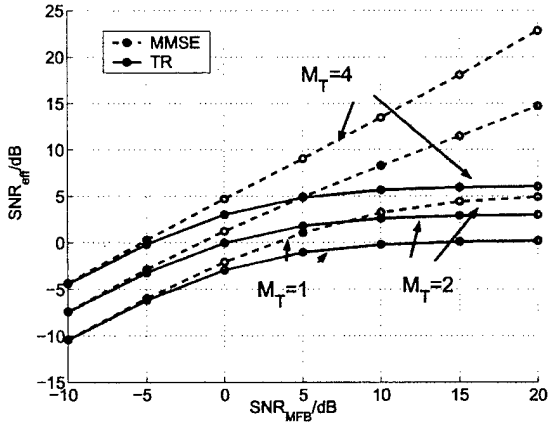

Fig. 19. The effective SNR increases with the number of transmit antennas.

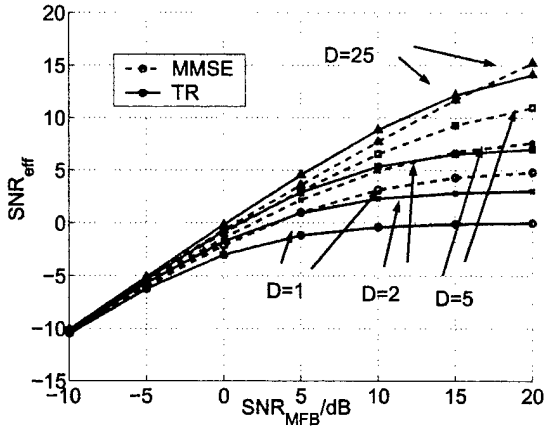

Fig. 20. Rate back-off improves the effective SNR.

achieve a transmission rate of 125 Mbps at 12 dB receive SNR with a single one-tap receiver and independent of the delay spread of the channel.

D. Performance Evaluation

We study the performance of the optimal and the TR prefilters in dependence on the number of transmit antennas and the rate back-off, and examine furthermore the variance of the received power as a function of bandwidth.

In Fig. 19 we plot the effective SNR of the two filters as a function of ρ_{MFB} ranging from -10 to 20 dB; in this picture, an optimal system would be characterized by a line with slope 1. The effective SNR is computed using 100 CIRs. The curves for the MMSE filter are dashed, those for the TR filter continuous. The three different curves for each filter are obtained for $M_T = 1, 2$, and 4. The results for the TR filter match the prediction of (47). For large ρ_{MFB}, the effective SNR becomes constant. It is 0 dB for $M_T = 1$, and increases with 3 dB for each additional transmit atenna. At low SNR, the curves increase linearly with ρ_{MFB}. In this range, the TR filter performance equals that of the MMSE filter. The effective SNR for the SISO system is quite bad; however, the shown performance is achieved with an extremely simple, one-tap receiver, and in a channel with very long delay spread. The optimized prefilter shows much better performance. For $M_T = 1$, the effective SNR saturates at a value which appears to depend on the delay spread of the channel and its correlation between taps. For more than one transmit antenna, the optimized prefilter can completely eliminate ISI, so that ρ_{eff} grows without bound. The slope of the curve depends on the number of transmit antennas. We believe it is interesting to study analytical expressions for the behavior of ρ_{eff} for the optimal prefilter in the limit of very large bandwidth.

The system can operate with rate back-off in order to increase the performance at the cost of transmission rate. The effective SNR for a single-antenna system with rate back-off of $D = 1, 2, 5$, and 25 is displayed in Fig. 20. It increases with decreased rate. Also, the saturation of the effective SNR sets in much later; the (almost) linear increase of ρ_{eff} reaches for the TR system with $D = 5$ up to $\rho_{MFB} = 10$ dB, and for one with $D = 25$ up to 15 dB. In this linear range, the performance of the TR prefilter is, in terms of the effective SNR, partly higher than that of the MMSE prefilter, since the latter is optimized for ISI suppression at $D = 1$ and has less power in its central peak. If the MMSE prefilter had been optimized for transmission with rate back-off, it would be at least as good as the TR prefilter. The design of such a prefilter could be interesting for preequalized wideband data transmission. When spectral efficiency has not highest priority, transmission rate back-off (while keeping the transmission bandwidth constant) is very efficient in order to improve system performance.

We characterize the fading of the channel, which we compute as the normalized variance of the instantaneous effective SNR,

$$\sigma^2_{SNR} = \mathrm{Var}\frac{P_{Tx}P_0}{P_{Tx}Q^{[D]} + \sigma^2} / E[\frac{P_{Tx}P_0}{P_{Tx}Q^{[D]} + \sigma^2}]^2. \quad (53)$$

We compute the variance for both filters for $\rho = 10$ dB and $M_T = 1$ in dependence on the number of taps of the channel. If the channel has only a few taps the peak of the preequalized CIR fades with higher probability than at high bandwidth with a large number of taps. The result is shown in Fig. 21 for the number of taps in the range between about 1 and 100. The shown curves are based on an average over 100 different realizations of the channel. We see that the variance decreases quickly with the number of taps; at only 20 taps it is already very low.

E. Bit-Error-Rates of the System

We plot the bit-error-rates (BERs) of the system, for rate back-offs of $D = 1, 2, 5$, and 25, i.e. the same as in Fig. 20. In Fig. 22 we show the BER of the TR (blue, cont.) and the MMSE (black, dashed) prefilter against SNR. Simulations were obtained from sending 5000 bits over 5000 different channels with $L = 100$. For $D = 1$ and also $D = 2$, BER of the TR prefilter floors quickly. For large rate back-off, BER is due to the increased effective SNR in the same range as that

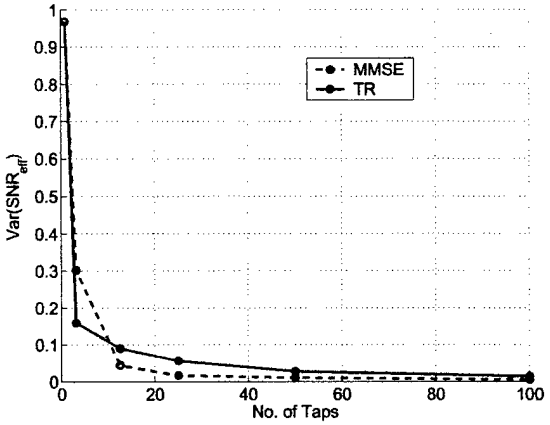

Fig. 21. The variance of the received signal decreases with increasing bandwidth.

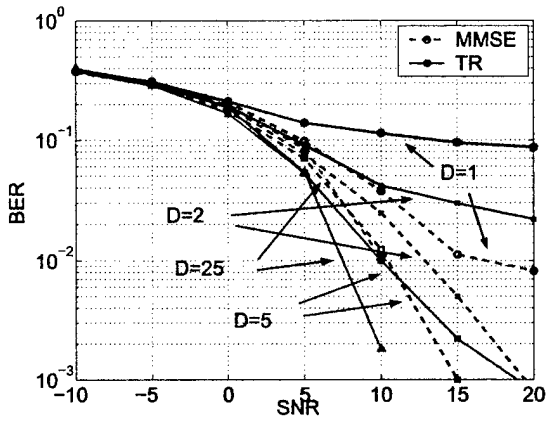

Fig. 22. The BER of the TR and the MMSE prefi lter.

of the MMSE prefilter for lower rate back-off. The TR system performs well for $D \geq 5$; the MMSE prefilter performs well for $D \geq 2$. For large D, both systems perform in general similarly well, since the MMSE filter was not optimizted for rate back-off. A worthwhile study would be the performance of a system equipped with a short MMSE equalizer at the receiver. The performance would potentially be much better and the rate back-off could be reduced even though only a simple receive equalizer was used.

VI. TR Channel Sounding

The value of TR for practical systems can only be assessed through experiments. In this section we describe how a channel sounder can be designed that can perform real-world TR experiments. This design does not require new technological concepts; we rather want to show how a conventional wideband MIMO sounder can be converted into a sounder for TR experiments. A more detailed version of the following can be found in [35].

A. Architecture

In TR experiments, one wants to demonstrate temporal and spatial focusing achieved in a wide band channel. In order to demonstrate temporal focusing, high resolution of the received CIR is required. To reveal spatial focusing, more than one receive antenna is necessary; one receive antenna is the one that receives the time compressed signal. At any other antenna, a noise-like signal will be visible. A wideband SIMO system is hence the minimum requirement to demonstrate TR. The key difference between between MIMO channel sounding and a TR experiment is that the latter requires CSI. The CSI must be updated in intervals the length of which depend on the Doppler spread of the channel. Since even comparably stationary channels as those for fixed wireless access can have a Doppler spread of more than 1 Hz [36], the CSI must be updated much faster than once per second and slow methods, like a frequency domain sweep measurement, are not useful. We will consider time- or frequency domain correlation methods, since they are both fast and can be used for wideband channel sounding.

In common correlation-based wideband channel sounding experiments, a transmitter transmits known sequences to a receiver. Transmitter and receiver are synchronized, and the receiver uses the received sequences in order to estimate the channel. In a TR experiment, the transmitter knows the channel, and convolves the transmit sequence with the time reversed CIR before transmission. The receiver uses again the received sequences to estimate the time-reversed channel, which will now exhibit spatial and temporal focusing. In order to convert a MIMO channel sounder into a TR channel sounder, CSI must be made available to the transmitter, and the transmitter must be able to convolve the CIR with the transmit sequence. Furthermore, the sounder must still be able to estimate the channel before CSI is fed into the transmitter.

A high-level sketch of a possible design is shown in Fig. 23. A MIMO channel sounder, which consists of an RF part for transmitter and receiver (RFTx and RFRx), a signal generator at the transmitter (SGTx) and a data storage unit at the recevier (DSRx) is equipped with a TR-signal processing unit (TRSPU). The main task of the TRSPU is to drive the estimiation of the CSI, and to transfer the CSI via the feedback loop to the transmitter, where the CIRs are convolved with the transmit sequence and transmitted over the channel. The details of the TRSPU and the feedback loop are explained in the next subsection.

B. TRSPU and Feedback Loop

A TR channel sounder operates in three steps, which are controlled by the TRSPU and shown in Fig. 24. In a first step, the channel is estimated between a given transmit antenna, say Tx_0, and a given receive antenna, Rx_0. This can be done by sending the known sequence $T(\omega)$, here expressed in frequency domain, n_1 times over the channel. Once the channel is estimated with some predefined accuracy, the estimated CSI $H_{0,0}$ is sent via the feedback loop to the transmitter. In a third step, the known transmit sequences $T(\omega)$ are multiplied with the estimated transfer function and transmitted into the

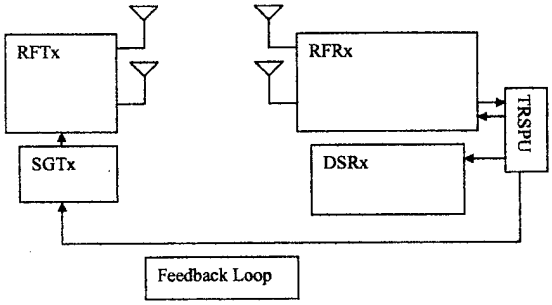

Fig. 23. A TR channel sounder can be designed using a MIMO channel sounder with a feedback loop for CSI.

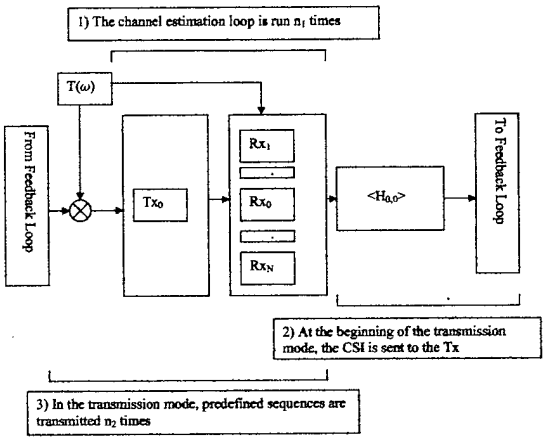

Fig. 24. The operational steps of a TR channel sounder.

channel. In this third step, the sounder switches between all its receive antennas. At Rx_0, it will receive a time reversed CIR; at all other antennas, it receives a noise-like signal. This time-reversed sequence can be sent n_2 times, until the CSI is outdated and the sounder has to start again with channel estimation.

Particular care is required for the choice of the feedback loop. The transferral time of the CSI must be much shorter than the coherence time of the channel. The data rate of the link becomes hence a critical parameter. A single complex CIR with about 1000 taps and 8 bit resolution has a size of about 16 kbit. Assuming a channel with Doppler frequency of 1 Hz, a realistic transmission time should not be longer than 0.2 s; consequently, the feedback loop needs a data rate of at least 80 kbit/s per CIR that is transferred.

The following options can be considered.

1) Microwave Link: A microwave link is advantageous in terms of data rate, which is in the order of Mbit/s, and in terms of flexibility. Microwave links can be established whereever the experiment is to be performed. However, TR experiments are likely to be conducted in environments with large delay spreads. The TR sounder will operate at maximum allowed EIRP. This limit holds for the microwave link, as well. In areas where the SNR of the TR experiment is low, that of the microwave feedback link is low, too. The link quality can be improved by using directional antennas mounted on high poles, but this requires difficult adjustments and large efforts in the preparation of the experiment.

2) Cellular Systems: Currently available cellular systems such as GPRS offer great flexibility without the need for heavy experimental equipment. Their main drawback is their comparably low data rate (order of 100 kbit/s for GPRS) and, in particular, the unreliable transmission delay. Since the data rate offered does not have too much overhead compared to the data rate required, the application of current cellular standards for the feedback loop appears risky in particular if the Doppler spread of the channel may at times exceed 1 Hz.

3) Ethernet: The ethernet offers tremendous data rates; its main drawback is the inflexibility of its access. However, most TR experiments will be conducted in urban areas, where access to the ethernet can be expected to be in range. A wireless network system such as one based on the IEEE 802.11b standard still offers data rates in the order of Mbits and can be employed to bridge the gap between the experimental device to the next ethernet connector.

The final decision about the best link depends on the availability of particular services, on local network traffic, and the Doppler spread of the channel.

C. Further Critical Specifications and Sources of Error

1) Range and Power: TR works best in environments with large delay spreads, i.e., large distances. Consequently, the demands on the link budget are high. Critical parameters which determine range are here pathloss exponent, maximum peak and average transmit power determined by hardware and regulations, bandwidth and carrier frequency, antenna gains, correlation gains, the sounder's sensitivity and target SNR.

2) Phase Noise: TR requires exact phase information at the transmitter. Inaccuracies in the phases occur since a) the channel is not perfectly time variant, b) the LO signals derived by PLLs from the (usually) 10 MHz reference have phase noise. The time variance can be overvome if the data rate of the feedback loop is large enough.

Phase noise destroys the coherent superposition of signals transmitted from multiple antennas. Since it enters both at the transmitter and the receiver, it will reduce the received power by a factor of $\cos(\Delta\phi_1 + \Delta\phi_2)$, where $\Delta\phi_i$, $i = 1, 2$ are random variables that describe the phase fluctuations of the transmitter's and the receiver's oscillators. For phase errors less than 15°, this yields a performance loss of about 10 % in SNR, which is tolerable.

VII. Conclusions and Outlook on Future Work

In this paper we introduced the concept and goals of time reversal (TR) techniques in the context of broadband wireless communications. TR by itself is a very simple preequalization scheme which moves the system's matched filter into the radio channel. When applied to wideband channels with very large delay spreads, this preequalizer very effectively captures the particular advantages of this channel, i.e. temporal and

spatial focusing as well as channel hardening. TR allows to shift complexity from transmitter to receiver and, thanks to its comparably low computational complexity, is likely to be a feasible scheme even if original channel impulse responses are very long.

We showed that the average rate of a TR scheme at low SNR is very close to the ergodic capacity of the frequency selective channel. In fading channels, the outage capacity can be improved if one transmits at higher bandwidth and exploits the channel hardening provided by TR.

Temporal and spatial focusing were investigated with three examples based on mesaured indoor UWB data, and on models of discrete and of continuous scattering. We illustrated how several proposed characterization metrics vary as a function of system and channel parameters, such as the bandwidth, delay and angle spreads, and number of antennas.

When addressing communication theoretic issues, only the most simple communication scheme with a single tap receiver has been considered. We saw that such a system can work in this harsh channel when the transmission bandwidth is sacrified for temporal/spatial focusing. More optimal transmission methods can achieve much better performance at the cost of more complexity at the transmitter.

Finally, we outlined how the TR channel can be measured with a system which is basically an upgraded commercially available MIMO channel sounder.

This overview touches many issues about transmission over channels with large delay spread for which TR is one potentially useful transmission scheme. Many questions have not been addressed. TR is optimal at very low SNR for very simple receivers. A natural question is to ask what happens if the receiver has more than just one tap, but still far not enough to equalize the channel on its own. It is not obvious that this problem results in a MMSE receiver, which could be used in combination with the TR precoder.

No space in this paper has been devoted to the analysis of a communication system that makes use of the spatial focusing properties of the proposed preequalization schemes. This topic is inherently connected to multiuser communications. The rate region of such a system requires the study of fading, frequency selective broadcast channels in the limit of large bandwidths. The derivation of optimal transmit and receive schemes would continue the work presented in this paper, or related work about joint transmit/receive optimization for multiuser communications but in the case of large delay spread. For TR, there appears to be a natural relation to the interference channel. In TR, the channel impulse response is temporally and spatially compressed solely with the knowledge of the channel of one individual link; no knowledge about the link to any other user or network is required. Hence, another potential application of TR is wideband networking with strong access points, architecturally very simple users, and a very low degree of cooperation.

A very critical aspect that has only briefly been discussed in Section VI is that of channel estimation. We believe that TR or any other preequalized system can be applied in TDD systems where the channel state information is estimated at the base station in the uplink, and then used in the downlink. That way, only the powerful base station needs to fully estimate the channel, and the handsets only estimate as many coefficients as the short length of their receive equalizers requires. In the uplink, no preequalization is performed, and the matched or any other receive filter is not in the channel, but in the receiver itself.

We believe that the study of communications over large bandwith / high delay spread channels is very fruitful. These channels offer potentially large rate, high diversity, and spatial and temporal focusing. TR systems that operate here provide a low-complexity solution for data transmission; their investigation may be a suitable starting point for more research in this area.

ACKNOWLEDGEMENT

The authors thank Intel Corp. / Santa Clara (CA, USA) for providing the measurement data used in the time reversal project. Claude Oestges is also pleased to acknowledge the financial support of the Belgian NSF.

REFERENCES

[1] A. Derode, P. Roux, and M. Fink, "Robust acoustic time reversal with high-order multiple scattering," *Phys. Rev. Letters*, vol. 75, pp. 4206–4209, 1995.

[2] M. Fink, "Time reversed acoustics," *Physics Today*, pp. 34–40, 1997.

[3] M. Fink, "Time-reversed acoustics," *Scientifi c American*, pp. 91–97, 1999.

[4] L. Borcea, G. Papanicolaou, and C. Tsogka, "Theory and applications of time reversal and interferometric imaging," to appear in *Inverse Problems*, 2004.

[5] D. R. Dowling and D. R. Jackson, "Phase conjugation in underwater acoustics," *J. Acoust. Soc. Am.*, vol. 89, pp. 171–181, 1990.

[6] D. R. Dowling and D. R. Jackson, "Narrow-band performance of phase-conjugate arrays in dynamic random media," *J. Acoust. Soc. Am.*, vol. 91, pp. 3257–3277, 1992.

[7] D. R. Dowling, "Acoustic pulse compression using passive phase-conjugate processing," *J. Acoust. Soc. Am.*, vol. 95, pp. 1450–1458, 1994.

[8] W. A. Kuperman, W. S. Hodgkiss, H. C. Song, T. Akal, C. Ferla, and D. R. Jackson, "Phase conjugation in the ocean: experimental demonstration of an acoustic time-reversal mirror," *J. Acoust. Soc. Am.*, vol. 103, pp. 25–40, 1998.

[9] W. S. Hodgkiss, H. C. Song, W. A. Kuperman, T. Akal, C. Ferla and D. R. Jackson, "A long-range and variable focus phase-conjugation experiment in shallow water," *J. Acoust. Soc. Am.*, vol. 105, pp. 1597–1604, 1999.

[10] S. Kim, G. F. Edelmann, W. A. Kuperman, W. S. Hodgkiss, and H. G. Song, "Spatial resolution of time-reversal arrays in shallow water," *J. Acoust. Soc. Am.*, vol. 110, pp. 820–829, 2001.

[11] D. Rouseff, D. R. Jackson, W. L. J. Fox, C. D. Jones, J. A. Ritcey and D. R. Dowling, "Underwater Acoustic Communication by Passive-Phase Conjugation: Theory and Experimental Results," *IEEE J. Ocean. Eng.*, vol. 26, pp. 821-831, 2001.

[12] M. G. Heinemann, A. Larazza and K. B. Smith, "Acoustic communications in an enclosure using single-channel time-reversal acoustics," *Appl. Phys. Lett.*, vol. 80, pp. 694–696, 2002.

[13] G. F. Edelmann, T. Akal, W. S. Hodgkiss, S. Kim, W. A. Kuperman and H. C. Song, "An initial demonstration of underwater acoustic communications using time reversal," *IEEE J. Ocean. Eng.*, vol. 27, pp. 602-609, 2002.

[14] P. Roux, B. Roman and M. Fink, "Time-reversal in an ultrasonic waveguide," *Appl. Phys. Lett.*, vol. 40, pp. 1811–1813, 1997.

[15] P. Roux and M. Fink, "Time reversal in a waveguide: Study of the temporal and spatial focusing," *J. Acoust. Soc. Am.*, vol. 107, pp. 2418–2429, 2000.

[16] A. Derode, A. Toupin, J. de Rosny, M. Tanter, S. Yon and M. Fink, "Taking advantage of Multiple Scattering to Communicate with Time-Reversal Antennas," *Phys. Rev. Letters*, vol. 90, 2003.

[17] T. Strohmer, M. Emami, J. Hansen, G. Papanicolaou and A. Paulraj, "Application of time-reversal with MMSE equalizer to UWB communications," to appear in *Proceedings of Globecom Conference 2004*, 2004.

[18] P. Kyritsi, G. Papanicolaou, P. Eggers and A. Oprea, "MISO time reversal and delay-spread compression for FWA channels at 5 GHz," *IEEE Antennas and Wireless Propagat. Lett.*, vol. 3, no. 6, pp. 96-99, 2004.

[19] Y. Chang, H.R. Fetterman, I.L. Newberg and S.K. Panaretos, "Microwave phase conjugation using antenna arrays," *IEEE Trans. Microwave Theory and Techniques*, vol. 46, no. 11, pp. 1910-1919, 1998.

[20] J. Tuovinen, G.S. Shiroma, W.E. Forsyth and W.A. Shiroma, "Multipath communications using a phase-conjugate array," *IEEE MTT-S Int. Microwave Symp. Digest*, vol. 3, pp. 1681-1684, 2003.

[21] F. Dietrich, R. Hunger, M. Joham and W. Utschick, "Linear precoding over time-varying channels in TDD systems," *IEEE International Conf. on Acoustics, Speech and Signal Processing ICASSP '03*, vol. 5, pp. 117-120, 2003.

[22] R. Esmailzadeh et al., "Prerake diversity combining in time-division duplex CDMA mobile communications," *IEEE Trans. Veh. Techn.*, vol. 48, no. 3, pp. 795-801, 1999.

[23] A. Scaglione, P. Stoica, S. Barbarossa, G. Giannakis and H. Sampath, "Optimal designs for space-time linear precoders and decoders," *IEEE Trans. Signal Proc.*, vol. 50, no. 5, pp. 1051-1064, 2002.

[24] G. Forney and M. Eyuboglu, "Combined equalization and coding using precoding," *IEEE Comm. Mag.*, vol. 29, no. 12, pp. 25-34, 1991.

[25] W. Hirt and J. Massey, "Capacity of the discrete-time Gaussian channel with intersymbol interference," *IEEE Trans. Info. Theory*, vol. 34, no. 3, pp. 380-388, 1998.

[26] D. Porcino and W. Hirt, "Ultra-wideband radio technology: potential and challenges ahead," *IEEE Commun. Mag.*, vol. 41, no. 7, pp. 66-74, 2003.

[27] C. Oestges, A.D. Kim, G. Papanicolaeou, A.J. Paulraj, "Characterization of space-time focusing in time-reversed random fields," *IEEE Trans. Antennas and Propagat.*, vol. 53, no. 2, 2005 (in press).

[28] S.M. Emami, J. Hansen, A.D. Kim, G. Papanicolaeou, A.J. Paulraj, D. Cheung, C. Prettie, "Predicted time reversal performance in Wireless Communications using channel measurements," *IEEE Comm. Letters* (in press).

[29] M. Emami, M. Vu, J. Hansen, G. Papanicolaou, and A. Paulraj, "Matched filtering with rate back-off for low complexity communications in very large delay spread channels," in *Proceedings of the Asilomar Conference 2004*, 2004, submitted.

[30] W.C.Y. Lee, *Mobile Communications Engineering*, McGraw-Hill, 1998.

[31] A. Paulraj, R. Nabar and D. Gore, *Introduction to Space-Time Wireless Communications*, Cambridge University Press, 2003.

[32] D.A. McNamara, C.W.I. Pistorius and J.A.G. Malherbe, *Introduction to the Uniform Theory of Diffraction*, Artech House, 1990.

[33] A. Ishimaru, *Wave propagation and scattering in random media (vol. 2)*, Academic Press, 1978.

[34] P. Blomgren, G. Papanicolaou and H. Zhao, "Super-resolution in time-reversal acoustics," *J. Acoust. Soc. Am.*, vol. 111, pp. 230–248, 2002.

[35] J. Hansen and A. Paulraj, "Design approach for a time reversal test bed for radio channels," in *Proceedings of the Eusipco 2004*, 2004, accepted.

[36] IEEE 802.16 Broadband Wireless Access Working Group, "The SUI channel models," Tech. Rep. IEEE 802.16.3c-01/29r5, 2003.

Predicted Time Reversal Performance in Wireless Communications Using Channel Measurements

S. M. Emami, *Student Member, IEEE*, J. Hansen, *Student Member, IEEE*, A. D. Kim, G. Papanicolaou, A. J. Paulraj, *Fellow, IEEE*, D. Cheung, and C. Prettie

ABSTRACT

Using broadband radio wireless measurements in an indoor environment we demonstrate the remarkable space-time focusing properties of signal transmission with time reversal.

I. INTRODUCTION

In a basic time reversal experiment, the intended receiver first broadcasts a short pilot pulse. The transmitter estimates the channel impulse response and sends the time reversed version of it back into the channel. These "time reversed" waves back propagate in the channel by retracing their paths and focus in space and time at the source, the intended receiver.

In a channel with rich scattering, multipath or multiple scattering is exploited by TR [1] to focus broadband signals tightly in space and time. Moreover, the effective channel obtained through TR is hardened or statistically stable [2]. Spatial focusing means that the spatial profile of the power peaks at the intended receiver and decays rapidly away from the receiver. Temporal focusing means that the channel impulse response at the receiver has a very short effective length. Channel hardening is the phenomenon of tightening of the distribution function of the effective channel impulse response. TR works well in systems where the delay spread of the channel times the bandwidth of the system is large [3], [2]. In this paper, we demonstrate TR with an Ultra-Wideband system in an indoor environment.

The use of TR has three main benefits in communications. Temporal focusing significantly shortens the effective length of the channel. For example, the complexity of a MLSE equalizer is exponential in the length of the channel. TR, thus, reduces the complexity of the equalization task.

A more important advantage of the TR technique is *spatial focusing* [2]. Spatial focusing results in very low co-channel interference in a multi-cell system. This results in a very efficient use of bandwidth in the overall system.

Another advantage of using TR is the hardening of the effective channel, which means that TR results in a high diversity gain. The statistics of the time reversed channel are different from the actual channel. Specifically the time reversed channel has a much smaller variance than the physical channel itself [2].

Fink and his coworkers [1], [3] (and references therein) have conducted an extensive number of experiments with TR in ultrasound and have shown large gains in spatial focusing in the presence of rich scattering. Also, TR methods have been used for underwater acoustic and ultrasound communications [4], [5], [6], [3]. TR experiments using radio waves rather than acoustic waves have not yet been done. Here, we shall perform an initial demonstration of the effects of TR methods applied to radio wireless measurements taken from an indoor environment in the band 2-8GHz. Based on these measurements, we predict the performance of TR in such a setting. We demonstrate temporal and spatial focusing for a SISO link and evaluate channel hardening in terms of the empirical distribution of the received signal strength. Our prediction of the TR performance is exact if there is no channel measurement error at the transmitter and any imperfections in the transmit and the receive chain of the system are not too severe.

In Section II we explain how data from static channel measurements can be used to predict the performance of a TR system, and we define suitable performance measures. In Section III we describe how the measurements were made. In Section IV we discuss the results and finally conclude with Section V.

II. TR FORMULATION

Consider a transmitter-receiver pair. In TR the transmitter uses the time reversed complex conjugate of the channel impulse response as the transmit prefilter. Denote the channel impulse response by $h(\mathbf{r_0}, \tau)$, where $\mathbf{r}_0$ is the receiver location and τ is the delay variable. If the transmitter uses $h^*(\mathbf{r_0}, -\tau)$ as the prefilter, the effective channel to any location $\mathbf{r}$ is thus given by the *time reversed field*:

$$s(\mathbf{r}, \tau) \triangleq \mathbf{h}^*(\mathbf{r_0}, -\tau) * \mathbf{h}(\mathbf{r}, \tau) \quad (1)$$

where $*$ denotes convolution with respect to delay. Note that a convolution with a time-reversed signal is equivalent to a correlation.

In order to study the effects of TR we measure the channel impulse response between the transmitter and a receiver. We repeat the measurement by holding the transmitter fixed and changing the position of the receiver over a square grid. We take one corner of the grid as the reference receiver (the

S. M. Emami, J. Hansen, and A. Paulraj are with the Integrated Systems Lab at Stanford University; A. D. Kim and G. Papanicolaou are with the Department of Mathematics at Stanford University, Stanford (CA), USA, E-mail: memami,jchansen,adkim,apaulraj,papanicolaou@stanford.edu. D. Cheung and C. Prettie are with Intel Corp., Santa Clara (CA), USA. Email: clifford.w.prettie,david.b.cheung@intel.com. Jan Hansen's work was supported by the Deutsche Forschungsgemeinschaft. This work is partially supported by grants AFOSR F49620-01-1-0465 and ONR N00014-02-1-0088.

intended receiver) and use its impulse response as the transmit prefilter $h^*(\mathbf{r_0}, -\tau)$. The time reversed field at any point on the square grid can now be computed based on the channel measurements and by using Eqn. 1. This is equivalent to having the transmitter perform the prefiltering with the TR filter.

The power of the signal as a function of both space and delay is computed and investigated. As a metric for spatial focusing we define the following quantity:

$$\kappa(\mathbf{r}) \triangleq \max_{\tau} |\mathbf{s}(\mathbf{r}, \tau)|^2 \qquad (2)$$

This quantity represents the power of the strongest tap at a receiver located at $\mathbf{r}$. We expect $\kappa(\mathbf{r})$ to peak at $\mathbf{r_0}$ and to decay rapidly with increasing distance from the origin.

III. Measurement Setup

Measurements were conducted by Intel Corporation at off-peak hours to ensure channel stationarity. The environment is an office space ($40m \times 60m$) with many cubicles. Measurements span the bandwidth 2-8 GHz with 3.75 MHz frequency resolution. From the data we estimate that the coherence bandwidth of the channel is 20 MHz Antennas are vertically polarized. The virtual grid on which the receiver is moved has a distance of $\lambda_0/4$ where λ_0 is the wave length of the mid frequency of the measurements (5 GHz).

The receive antenna is moved to a different location with a precise robotic positioner. At each antenna position, the channel is measured using a vector network analyser. The measurements are corrected to compensate for the system components (including cable, gain stages, and antennas). The height of the transmit antenna is about 2.5m and that of the receive antenna is 1m above the floor. The channel impulse response was computed by taking the inverse DFT of measurement data.

IV. Experimental Results

We evaluated $\kappa(\mathbf{r})$ for 11 different scenarios. Here we present two cases. Case I is an essentially line-of-sight scenario with a separation of 3m. Case II has a separation of 11m and is a typical non-line-of-sight situation. The results for the two cases discussed here have the worst focusing and yet they are very similar in their outcomes with all the other scenarios.

In the 3-D figures, the square grid spans a region of $7\lambda_0 \times 7\lambda_0$. A 3D plot of $\kappa(\mathbf{r})$ of the two cases is shown in Fig. 1. We see that spatial focusing works fine in both scenarios. In neither of them, however, the peak is isotropic; both peaks have one direction in which they fall off faster, and another, in which the decay is slower. The structure of the peak carries some information about the geometry of the environment, i.e., about directions which show faster and those which show slower decorrelation in space.

We also observe that the signal power level is at least $10dB$ lower at a distance of $7\lambda_0$ than its value at the receiver. This demonstrates the spatial decorrelation very well. We can conclude that channel impulse responses show inherent quasi-orthogonality in space, which can be used for interference suppression. In Fig. 2 we demonstrate the compression of the

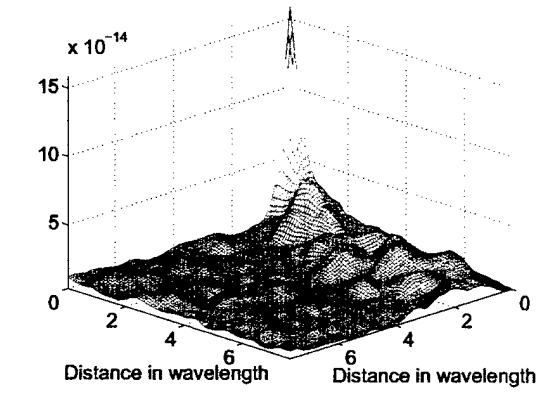

(a) Case I

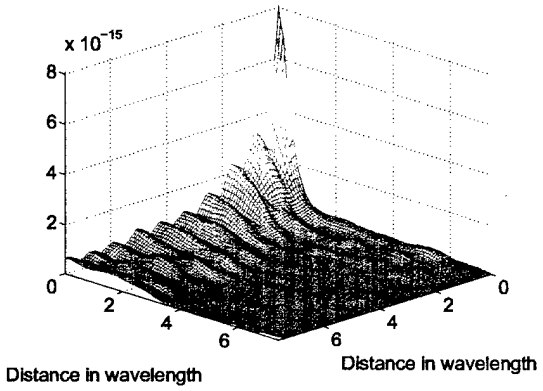

(b) Case II

Fig. 1. Spatial Focusing $\kappa(\mathbf{r})$. One shot spatial field realizations for a) the line-of-sight b) the non-line-of-sight scenario.

received pulse in the time domain. Displayed are the channel impulse response magnitude for the LOS scenario (a), the respective time-reversed, i.e., compressed impulse response magnitude (b), the impulse response for the NLOS scenario (c), and the compressed one for this case (d). The effective length of the channel is significantly shortened. Still, for the LOS-case, comparably strong side lobes remain visible. The impulse response of the NLOS channel is much better compressed in time. There is some intersymbol interference in the time compressed field and one would need to equalize the received signal. However, the time compressed channel has a significantly shorter effective length and is thus less expensive to equalize.

In Fig. 3 we investigate the hardening of the channel. We consider the distribution of the strongest tap of the channel impulse response and of time-reversed field. The dashed curve represents the distribution of the zero-th tap of the channel impulse response, and the solid curve represents that of the compressed signal. The figure illustrates that the time reversed

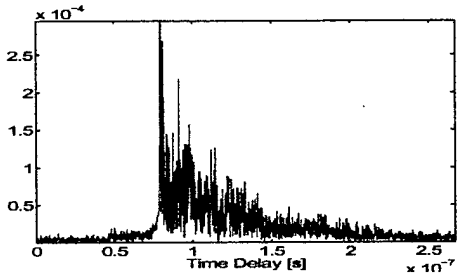

(a) Case I

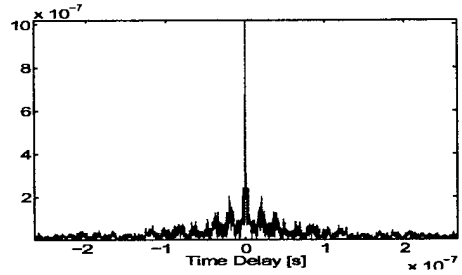

(b) Case I

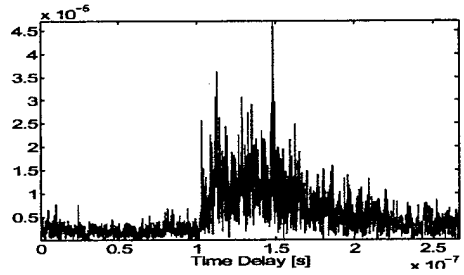

(c) Case II

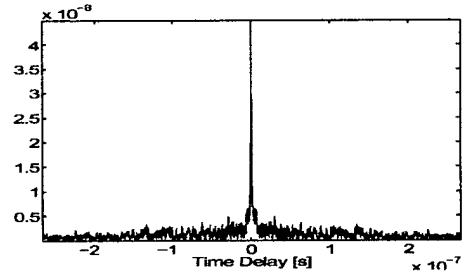

(d) Case II

Fig. 2. Magnitude of channel impulse responses (a and c) and the time compressed impulse response (b and d)

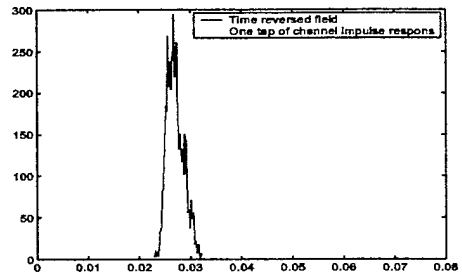

Fig. 3. Distribution of $s(\mathbf{r},0)$ (solid) and that of $h(\mathbf{r},0)$

field is much less random (i.e., has more diversity) than the channel response itself.

V. Conclusions

Using the indoor measurements discussed above, TR results in strong spatial focusing and time compression. At about 7 wavelengths from the target the signal power reduces by at least $10dB$ from its value at the target. The channel impulse response is well shortened at the target as well. Channel hardening or diversity gain is also observed. In a practical setting the results may degrade if the transmitter does not perfectly know the channel or if the transmitter circuitry has nonlinearities. Our calculations with the indoor radio wireless measurements obtained by Intel suggest that the benefits of TR, which have been observed in ultrasound and underwater sound TR experiments, could also be gained in wireless communications.

References

[1] A. Derode, P. Roux, and M. Fink, "Robust acoustic time reversal with high-order multiple scattering," *Phys. Rev. Letters*, vol. 75, pp. 4206–4209, 1995.

[2] L. Borcea, G. Papanicolaou, and C. Tsogka, "Theory and applications of time reversal and interferometric imaging," *Inverse Problems*, vol. 19, pp. 5139–5164, 2003.

[3] A. Derode *et al.*, "Taking advantage of multiple scattering to communicate with time-reversal antennas," *Phys. Rev. Letters*, vol. 90, pp. 014 301–1–014 301–4, 2003.

[4] D. Rouseff *et al.*, "Underwater acoustic communication by passive-phase conjugation: Theory and experimental results," *IEEE Journal of Oceanic Engineering*, vol. 26, pp. 821–831, 2001.

[5] M. G. Heinemann, A. Larazza, and K. B. Smith, "Acoustic communications in an enclosure using single-channel time-reversal acoustics," *Appl. Phys. Lett.*, vol. 80, pp. 694–696, 2002.

[6] G. F. Edelmann *et al.*, "An initial demonstration of underwater acoustic communications using time reversal," *IEEE Journal of Oceanic Engineering*, vol. 27, pp. 602–609, 2002.